

ANALYSIS OF INITIAL AND FINAL STATE INTERACTIONS
IN QUANTUM CHROMODYNAMICS*

Geoffrey T. Bodwin
Stanford Linear Accelerator Center
Stanford University, Stanford, California 94305

Stanley J. Brodsky
Institute for Advanced Study
Princeton, New Jersey 08540
and
Stanford Linear Accelerator Center[†]
Stanford University, Stanford, California 94305

and

G. Peter Lepage[‡]
Institute for Advanced Study
Princeton, New Jersey 08540
and
Laboratory of Nuclear Studies[†]
Cornell University, Ithaca, New York 14853

(Submitted to Physical Review D)

*Work supported by the Department of Energy, contract DE-AC03-76SF00515.

[†]Present address.

[‡]Work supported by the National Science Foundation.

ABSTRACT

We demonstrate that the standard factorization theorem for the Drell-Yan process and other hadron-induced hard-scattering inclusive reactions is violated order by order in QCD perturbation theory by initial state interactions. The initial state effects occur in leading order in $1/s$ and come from the near-on-shell scattering region, whose contributions cannot be eliminated by the use of Ward identities. Because of the large longitudinal range of the initial state interactions, the lepton-pair cross section is not additive in the nucleon number of the target. At asymptotic Q^2 , the factorization-violating initial state effects are suppressed if one sums certain hard-scattering radiative corrections to all orders in perturbation theory. We also discuss the concept of the formation zone in QCD, and show that collinear radiation cannot be induced inside a target whose length is shorter than a scale proportional to $1/s$. In general, initial and final state interactions in QCD lead to a number of new observable phenomena, including induced color correlations, k_{\perp} fluctuations, and radiation in the central region. The initial and final state effects vanish in leading order in $1/s$ for hard-scattering exclusive processes and certain semi-inclusive direct processes.

I. INTRODUCTION

Recently we have shown that initial state interactions have a significant effect on almost any hard inclusive or semi-inclusive cross section for hadron-hadron scattering, including the Drell-Yan process ($pp \rightarrow \mu\bar{\mu}X$), hadronic jet production ($pp \rightarrow q\bar{q}X$), and inclusive η_c production ($pp \rightarrow \eta_c X$).¹ Not only do these initial state effects invalidate previous analyses of such processes, but they lead to a host of new phenomena, many of which are experimentally accessible. Such initial state interactions are intimately related to the final state interactions that change quark and gluon jets into hadron jets in processes like $e\bar{e} \rightarrow \text{hadrons}$ and $ep \rightarrow e + \text{hadrons}$. Thus, Drell-Yan and similar reactions provide an important new tool for studying these little-understood aspects of the strong interaction. In this paper we examine the qualitative features of initial and final state interactions in quantum chromodynamics, focusing on the example of the Drell-Yan process and using perturbation theory as a guide. The phenomenological implications for Drell-Yan, deep inelastic scattering, and a variety of other processes will be explored in a subsequent paper.

In order to illustrate the issues, let us consider the Drell-Yan process $\pi A \rightarrow \bar{\mu}\mu X$ where an anti-quark in the pion annihilates on a quark in nucleus A. In conventional analyses, based upon the parton model² and QCD factorization 'theorems',³ one ultimately computes only interactions involving the annihilating (or 'active') quark and anti-quark. Then the Drell-Yan cross section has the factorized form shown in Fig. 1: a convolution of structure functions for the beam and target particles with a (hard) $q\bar{q}$ annihilation cross section. The $q\bar{q}$ cross section is calculable in perturbation theory, and the structure functions can be measured in deep

inelastic scattering. Thus both the Q_{\perp} distribution of the $\mu\bar{\mu}$ pairs and the normalization of the integrated cross section $d\sigma/dQ^2 dx_F$ are completely determined for large pair mass Q^2 . Furthermore, if one assumes that the factorization theorems are valid, then the cross section for nuclear targets scales simply as A^1 ; the nucleus is effectively transparent to the active beam quark, allowing the quark to annihilate on any nucleon in the nucleus.

Here we show this picture is incomplete. In fact, the active quark and anti-quark suffer any number of glancing collisions with the various spectator partons before annihilating (Fig. 2). These initial state interactions can profoundly alter the character of the process. It is sometimes argued that such interactions are negligible in the high energy limit because the time available vanishes as $s \rightarrow \infty$ due to Lorentz contraction of the beam and target particles (in the center of mass frame). This argument ignores the fact that the probability amplitude for scattering grows like $T \sim s$ in theories with vector exchange 'particles' — e.g., gluons, photons, pomerons. As we shall show, initial state interactions occur at large s for just this reason — although only between beam and target constituents. The quarks and gluons within the pion, for example, have no time to interact with each other during their passage through the nucleus.

Initial state effects are, perhaps, most easily observed in the transverse momentum of the lepton pair.⁴ The initial state collisions transfer only limited momentum in the $s \rightarrow \infty$ limit. Thus, they have a negligible effect upon the longitudinal momenta of the annihilating quarks, but provide an important new source of transverse momentum for the quarks. This additional transverse momentum is potentially comparable in magnitude to the 'primordial p_T ' that originates in the hadron wave functions.

The quarks' transverse momentum is passed on to the $\mu\bar{\mu}$ pairs and is reflected in a broadened Q_{\perp} distribution for the pairs. This broadening is A dependent for nuclear targets, because the number of initial state collisions grows with target length (i.e., like $A^{1/3}$). The transverse momentum of the active anti-quark in the pion fluctuates randomly as the anti-quark collides with the various nucleons comprising the nucleus. This increases the mean Q_{\perp}^2 of the $\mu\bar{\mu}$ pair by

$$\delta\langle Q_{\perp}^2 \rangle \sim A^{1/3} \lambda^2, \quad (1.1)$$

where λ is the typical momentum transfer per collision ($\lambda \sim 100$ to 500 MeV). There is already some indication in the data for such an A-dependent shift in $\langle Q_{\perp}^2 \rangle$ (see Fig. 3).⁵

If the initial state interactions are both color and flavor neutral, their sole effect for large s and Q^2 is to broaden the Q_{\perp} distribution. The cross section $d\sigma/dQ^2 dx_F$ (integrated over Q_{\perp}) is unchanged because it is insensitive to the limited transfers of momentum involved. This is easily understood from our analysis: in spite of initial state collisions, quark flux is conserved in the beam direction since the momenta and trajectories of the active quarks are essentially unchanged. The net effect, then, is to change the active quark and anti-quark wave functions by a unitary eikonal phase⁶ $U(b_{\perp})$ that varies with their impact parameters. Although this phase obviously modifies the transverse momentum dependence, it cancels in the integrated cross section:

$$\frac{d\sigma(\pi A \rightarrow \mu\mu X)}{dQ^2 dx_F} \sim \int d^2b_{\perp} \langle \pi A | U^{\dagger}(b_{\perp}) \mathcal{M}^{\dagger}(q\bar{q}) \mathcal{M}(q\bar{q}) U(b_{\perp}) | \pi A \rangle \quad (1.2)$$

$$= \int d^2b_{\perp} \langle \pi A | \mathcal{M}^{\dagger}(q\bar{q}) \hat{\mathcal{M}}(q\bar{q}) | \pi A \rangle, \quad ,$$

where $\mathcal{M}(q\bar{q})$ is the amplitude for $q\bar{q}$ annihilation, and $U^{\dagger}U = 1$.

The situation is radically different when the initial state interactions transfer color, as must be the case in QCD. Although quark flux along the beam is always conserved, the color wave functions of the active quarks are changed by the gluon exchanges. In the conventional picture, the active quark and anti-quark do not communicate until they annihilate, and consequently their colors are uncorrelated. As a result, the Drell-Yan cross section is reduced by a factor of 1/3 compared to the colorless case, since two times out of three the quark and anti-quark colors do not match. Initial state collisions involving color exchange can introduce color correlations, dramatically affecting the normalization even of the integrated cross section $d\sigma/dQ^2 dx_F$. This is evident from Fig. 4, which shows the dominant color flow due to the exchange of a single gluon before the annihilation. With this color flow, annihilation can always occur, no matter what the initial colors of the quarks. Thus, the eikonal operator U can no longer be neglected in Eq. (1.2). Although $U^\dagger U = 1$ (flux conservation), the eikonal is a color matrix in QCD and no longer commutes with the $q\bar{q}$ annihilation amplitude $\mathcal{M}(q\bar{q})$. This is an essential difference between deep inelastic scattering and the Drell-Yan process. In deep inelastic scattering the eikonal appears only in the final state and always cancels, by unitarity, in the cross section (cf Eq. (1.2)):

$$\begin{aligned} \frac{d\sigma(eA \rightarrow eX)}{dQ^2 dx} &\sim \int d^2b \langle A | \mathcal{M}^\dagger(eq) U(b_\perp) U^\dagger(b_\perp) \mathcal{M}(eq) | A \rangle \\ &= \int d^2b \langle A | \mathcal{M}^\dagger(eq) \mathcal{M}(eq) | A \rangle \quad . \end{aligned}$$

That is, $\mathcal{M}(eq)$, the amplitude for $eq \rightarrow eX$, need not commute with $U^\dagger(b_\perp)$, the eikonal operator, in order for final state interactions (Abelian

and non-Abelian) to be negligible. (See Appendix A for a more detailed illustration.)

In order to describe the color correlation effect in Drell-Yan in a more quantitative way, we decompose the general cross section for $q\bar{q}$ annihilation (i.e., $\mathcal{M}^\dagger \mathcal{M}$) into two components, corresponding to different color flows in the hard subprocess (Fig. 5):

$$d\sigma_{ac,bd}(q\bar{q} \rightarrow \mu\bar{\mu}X) = \frac{\delta_{ab}\delta_{cd}}{n_c} d\sigma_1 + 2(T^i)_{ba}(T^i)_{cd} d\sigma_8 \quad (1.3)$$

where a, \dots, d are color indices, $n_c = 3$, and the T^i are the generators of color transformations in the fundamental representation ($\text{Tr}(T^i T^j) = \delta_{ij}/2$). In the conventional analysis, the effective $q\bar{q}$ cross section is obtained by color averaging,

$$d\sigma_{\text{eff}} = \frac{1}{n_c^2} \sum_{a,c} d\sigma_{ac,ac} = \frac{1}{n_c} d\sigma_1 \quad (1.4)$$

and $d\sigma_8$ does not contribute since $\text{Tr}(T^i) = 0$. However, color changing initial state interactions can result in any (normalized) mixture of color states for the $q\bar{q}$. If $\cos^2\theta$ is the probability of finding the $q\bar{q}$ in a singlet after initial state collisions, then the effective annihilation cross section is⁷

$$d\sigma_{\text{eff}}(q\bar{q} \rightarrow \mu\bar{\mu}X) = \frac{1}{n_c} d\sigma_1 + \left(n_c \cos^2\theta - \frac{1}{n_c}\right) d\sigma_8, \quad (1.5)$$

where now $d\sigma_8$ ($\leq d\sigma_1$) contributes. An entirely new (color) channel is available for the Drell-Yan process. The mixing angle θ is determined by low momentum transfer initial state interactions, and as such cannot be computed perturbatively.

In lowest order perturbation theory, $d\sigma_8$ equals $d\sigma_1$ and so we find that

$$0 \leq d\sigma_{\text{eff}}(q\bar{q} \rightarrow \mu\bar{\mu}X) \leq n_c^2 \left(\frac{d\sigma_1}{n_c} \right) \quad (1.6)$$

- i.e., due to the color correlation effect, the Drell-Yan cross section could be enhanced by as much as a factor of 9 relative to the conventional result! However, as emphasized by Mueller,⁸ perturbative QCD suggests that $d\sigma_8$ is suppressed relative to $d\sigma_1$ by a quark form factor:

$$d\sigma_8 \sim d\sigma_1 \exp \left\{ - \frac{C_A}{\beta_0} \ln \left(\frac{\ln Q^2/\Lambda^2}{\ln \lambda_A^2/\Lambda^2} \right) \ln Q^2/\lambda_A^2 \right\} \quad (1.7)$$

$$\sim d\sigma_1 \times \begin{cases} \frac{1}{3} & Q^2 = 10 \text{ GeV}^2 \\ \frac{1}{10} & Q^2 = 100 \text{ GeV}^2 \end{cases}$$

where $C_A = n_c = 3$, $\beta_0 = 11 - 2/3 n_{\text{flavor}}$, $\Lambda \sim 100 \text{ MeV}$ is the QCD scale parameter, and $\lambda^2 = \lambda_A^2/\Lambda^2 \sim (100-500 \text{ MeV})^2$ is the square of the typical momentum transferred per initial state collision. This form factor is absent in $d\sigma_1$ because of a cancellation between real and virtual gluon emission. However, gluon radiation is strongly suppressed in $d\sigma_8$ (i.e., by a factor $1/(n_c^2 - 1)$) and the cancellation is spoiled. The detailed behavior of the form factor depends in part upon the low energy structure of QCD and may not be calculable at present. However, the form factor almost certainly vanishes as $Q^2 \rightarrow \infty$, so that $d\sigma_8$ can be ignored for very large $Q^2 (>> 100 \text{ GeV}^2)$, and the conventional result becomes valid - i.e., $d\sigma_{\text{eff}} \rightarrow 1/n_c d\sigma_1$. Based on the estimate given in Eq. (1.7), this is evidently not the case at current energies. Indeed, the Q^2 dependence of $d\sigma_8$ is an important new source of scaling violation, and possibly even the dominant source given the small values of $\Lambda_{\overline{\text{MS}}} (\lesssim 200 \text{ MeV})$ obtained from recent measurements. This Q^2 dependence is quite different

from scaling violation due to conventional structure function evolution, since the effective anomalous dimension of $d\sigma_8$ varies with Q^2 ; e.g., $\gamma_{\text{eff}} = -C_A/\beta_0 \ln Q^2/\lambda^2$ in perturbation theory.

The appearance of Sudakov double logarithms, which exponentiate to give the form factor in Eq. (1.7), signals the failure order by order in perturbation theory of the QCD factorization 'theorems'³ for Drell-Yan; mass singularities cannot be simply factored. Only when working to all orders do we recover the familiar results, and then only for Q^2 very large. This infrared sensitivity in leading twist was completely unexpected from previous analyses. In covariant and noncovariant gauges alike, it results from the failure of collinear Ward identities in the eikonal region of phase space, where gluons transfer infinitesimal fractions ($\sim\lambda^2/s$) of the longitudinal momentum carried by the beam and target particles (see Appendix A).

Flavor changing initial state interactions also affect the Drell-Yan cross section. As an extreme example, consider a Drell-Yan process for two mesons whose valence quarks are $\bar{s}d$ and $c\bar{u}$. If we neglect sea quarks, the process cannot proceed at all without an initial state interaction; W-boson exchange between an active quark and a spectator quark (Fig. 6) leads to a small, but non-zero Drell-Yan cross section even as $s \rightarrow \infty$.

An intriguing and important feature of the initial state (and final state) interactions is their range. Despite the Lorentz contraction of the beam and target particles in the center of mass frame, the longitudinal range of the interactions grows like \sqrt{s} in this frame (see Appendix B). Thus, in $\pi A \rightarrow \mu\bar{\nu}X$, for example, the beam antiquark interacts with the entire nucleus, even if the annihilation is at the front face. The mixing angle θ in Eq. (1.5) is then A dependent. However, a large n_c analysis

in QCD suggests that this dependence is suppressed by a factor $1/n_c^2$ and, therefore, that nuclear cross sections for Drell-Yan could still scale roughly as A^1 .

Central to the entire analysis outlined above is the fact that the longitudinal momenta of the active quarks are unchanged by initial state eikonal collisions. However, even the softest of collisions between high energy quarks can induce gluonic bremsstrahlung carrying off large fractions of the quarks' longitudinal momenta. Such radiation, if it could occur in an initial state collision in Drell-Yan, would greatly soften the quark x -distributions, thereby substantially reducing the cross section at a given Q^2 and x_F , and destroying any semblance of factorization. In fact, there is insufficient time for such collinear bremsstrahlung to develop during the collision of the hadrons, provided that

$$Q^2 \gg x M_N L_T \lambda^2 A^{1/3} \quad , \quad (1.8)$$

where x is the target quark momentum fraction, λ the typical momentum transfer per collision, M_N the nucleon mass, and L_T the target length. This condition is easily satisfied for a proton target, but somewhat larger Q^2 may be required for large nuclei (e.g., $Q^2 \gg x(24 \text{ GeV}^2)$ for uranium). It is also apparent from this condition that hadronic radiation is inevitable as the beam passes through any macroscopic target — a fact well appreciated by experimenters.

Initial state interactions do create central region particles, carrying limited longitudinal momentum, even when condition (1.8) is satisfied. These interactions tend to destroy the coherence of the active quark wave functions, thereby diminishing the Drell-Yan cross section. However, their effect is negligible provided that

$$\frac{Q^2}{x_q x_{\bar{q}}} \gg (M_{NN})^2 \lambda^2 A^{2/3} . \quad (1.9)$$

Notice that the central region multiplicity produced by these interactions should grow with increasing nucleon number like $A^{1/3}$.

The initial (and final) state interactions of interest here involve small momentum transfer, and therefore depend critically upon the non-perturbative behavior of QCD. Nevertheless, such effects do appear in perturbation theory, and a complete perturbative analysis leads to important insights into the qualitative features of these phenomena. Therefore, in the remainder of this paper, we outline the analysis of initial state corrections for $qA \rightarrow \mu\bar{u}X$, working to all orders in perturbation theory (A can be a meson, baryon, nucleus, ...). These corrections are most easily studied using time ordered perturbation theory in the center-of-mass frame⁹ - i.e.,

$$P_q = (P, 0_{\perp}, P)$$

$$P_A = (P, 0_{\perp}, -P)$$

with $s = 4P^2 \rightarrow \infty$ and masses set to zero. The time orderings of the diagrams are closely related to the path orderings that appear in the eikonal phases. This feature is particularly useful in separating initial from final state effects. We work in Coulomb gauge so as to avoid spurious collinear singularities, which can be confused with initial state effects when covariant gauges are used.

We proceed in two steps. First we examine the Drell-Yan process in the absence of gluonic radiation (Section II). Here we demonstrate the eikonalization of the initial state interactions and discuss their effects upon the Q_{\perp} -distribution and the normalization of the hadronic

process. We then include gluonic radiation (both real and virtual) and examine scaling violations in the Drell-Yan process, given the presence of soft interactions between the initial particles (Section III).

Finally, we summarize the phenomenological consequences of initial and final state interactions in Drell-Yan and other processes (Section IV).

The analysis of initial state interactions in covariant gauges is discussed briefly in Appendix A, where we also address the discrepancy between our results and those of Collins et al.¹⁰ The range of the eikonal potential and its relation to zitterbewegung is discussed in Appendix B.

II. INITIAL STATE COLLISIONS WITHOUT RADIATION

If we ignore both initial state collisions and radiation, the amplitude for $qA \rightarrow \mu\bar{\mu}X$ is (Fig. 7a)¹¹

$$\mathcal{M}_{DY}^0 = \frac{\mathcal{M}_H(q\bar{q} \rightarrow \mu\bar{\mu})}{x} \psi_A(x, k_\perp) = \int d^2 z_\perp \frac{\mathcal{M}_H}{x} e^{ik_\perp \cdot z_\perp} \tilde{\psi}_A(x, z_\perp) \quad , \quad (2.1)$$

where for simplicity we take A to be just a $q\bar{q}$ bound state. The (active) anti-quark in A has momentum $k = (k_\perp, -xP)$, with impact parameter z_\perp conjugate to k_\perp . Thus the lepton pair has mass $Q^2 = 4xP^2$, $Q_\perp = k_\perp$, and $x_F = 1-x$. At this stage the cross section still factors in the usual fashion:

$$\frac{d\sigma_{DY}^0}{dQ^2 dx_F} = \int dx G_A(x) \frac{d\sigma_{eff}}{dQ^2 dx_F} (q\bar{q} \rightarrow \mu\bar{\mu}) \quad , \quad (2.2a)$$

where $G_A(x)$ is a structure function,

$$G_A(x) = \frac{1}{x} \int \frac{d^2 k_\perp}{16\pi^3} |\psi_A(x, k)|^2 = \frac{1}{4\pi x} \int d^2 z_\perp |\tilde{\psi}_A(x, z_\perp)|^2 \quad (2.2b)$$

and $d\sigma_{eff} = (1/n_c) d\sigma_1$ (Eq. (1.4)).

This simple picture is complicated by initial state collisions. For example, the Abelian Coulombic interaction shown in Fig. 7b gives an amplitude

$$\begin{aligned}
 M_{DY}^{1c} \approx M_H \int \frac{d^3 \ell}{(2\pi)^3} \frac{1}{-2\ell^3 - \frac{(k_\perp - \ell_\perp)^2}{2(x+y)P} - \frac{\ell^2}{2(1+y)P} - \frac{k_\perp^2}{2(1-x)P} + i\epsilon} \\
 \times \frac{1}{2(1+y)P} \left(\frac{g^2 4P^2 (1-x+y/2)(1+y/2)}{\vec{\ell}^2} \right) \frac{\psi(x+y, k_\perp - \ell_\perp)}{2P(x+y)(1-x-y)}, \quad (2.3)
 \end{aligned}$$

where $\vec{\ell} = (\ell_\perp, yP)$ and we have neglected ℓ_\perp, k_\perp relative to P . Notice that in this gauge the collinear region $y \sim 1$ is suppressed by $1/s$. The only important contribution comes from the "Glauber region"¹² $\vec{\ell}^2 \sim \lambda^2$, where $\lambda^2 \sim \langle k_\perp^2 \rangle$ in ψ_A . Therefore as $P \rightarrow \infty$, we can neglect y relative to x and simplify the energy denominator to obtain an eikonal form for (2.3):

$$\begin{aligned}
 M_{DY}^{1c} &\approx \frac{M_H}{x} \int \frac{d^3 \ell}{(2\pi)^3} \frac{1}{-2\ell^3 + i\epsilon} \frac{g^2}{\vec{\ell}^2} \psi_A(x, k_\perp - \ell_\perp) \quad (2.4) \\
 &\approx \frac{M_H}{x} \int d^2 z_\perp \int_{-\infty}^0 \frac{d\tau}{i} \int \frac{d^3 \ell}{(2\pi)^3} e^{-i\tau(-2Q^3 + i\epsilon)} e^{-i\ell_\perp \cdot z_\perp} \\
 &\quad \times \frac{g^2}{\vec{\ell}^2} e^{ik_\perp \cdot z_\perp} \tilde{\psi}_A(x, z_\perp) \\
 &\approx \frac{M_H}{x} \int d^2 z_\perp \left\{ \int_{-\infty}^0 \frac{d\tau}{i} V(\vec{z}_\perp + \tau\vec{\Delta}) e^{\epsilon\tau} \right\} e^{ik_\perp \cdot z_\perp} \tilde{\psi}_A(x, z_\perp)
 \end{aligned}$$

where here V is just the Coulomb potential, $\vec{z}_\perp = (z_\perp, 0)$ and $\vec{\Delta} = (\vec{P}_A - \vec{P}_q)/P = (0_\perp, -2)$. Using similar arguments, we find the double Coulomb interaction (Fig. 7c) gives

$$\begin{aligned}
 \mathcal{M}_{DY}^{2c} &\approx \frac{\mathcal{M}_H}{x} \int \frac{d^3 \ell'}{(2\pi)^3} \int \frac{d^3 \ell''}{(2\pi)^3} \frac{1}{-2\ell'^3 - 2\ell''^3 + i\epsilon} \frac{g^2}{\ell'^2} \frac{1}{-2\ell'^3 + i\epsilon} \frac{g^2}{\ell''^2} \\
 &\times \psi(x, k_\perp - \ell_\perp - \ell'_\perp) \\
 &\approx \frac{\mathcal{M}_H}{x} \int d^2 z_\perp \left\{ \int_{-\infty}^0 \frac{d\tau}{i} V(\vec{z}_\perp + \vec{\Delta}\tau) e^{\epsilon\tau} \right. \\
 &\times \left. \int_{-\infty}^{\tau} \frac{d\tau'}{i} V(\vec{z}_\perp + \vec{\Delta}\tau') e^{\epsilon\tau'} \right\} e^{ik_\perp \cdot z_\perp} \tilde{\psi}_A(x, z_\perp) .
 \end{aligned}$$

For any number of interactions we obviously obtain

$$\begin{aligned}
 \mathcal{M}_{DY}^c &= \mathcal{M}_{DY}^0 + \mathcal{M}_{CY}^{1c} + \mathcal{M}_{DY}^{2c} + \dots \\
 &= \frac{\mathcal{M}_H}{x} \int d^2 z_\perp U(z_\perp) e^{ik_\perp \cdot z_\perp} \tilde{\psi}_A(x, z_\perp)
 \end{aligned}$$

in place of Eq. (2.1), where the (unitary) eikonal phase U is a path ordered exponential:

$$U(z_\perp) = \mathcal{P}_\tau \exp \left\{ -i \int_{-\infty}^0 d\tau V(\vec{z}_\perp + \vec{\Delta}\tau) \right\} . \quad (2.5b)$$

Equation (2.5) is easily understood in physical terms. The eikonal phase U is the probability amplitude for the beam quark to arrive at the annihilation point after repeated soft collisions with the spectator. The quark remains near mass-shell between collisions as it passes through A. (In Eq. (2.4), only the imaginary part of the energy denominator contributes, implying on-shell propagation. This is the origin of the 'i' in (2.5b).) The variable τ may be thought of as time, and the integral in (2.5b) as an integral over the classical trajectory of the beam quark through the target up to the annihilation at $\tau = 0$. $|\vec{z}_\perp + \tau\vec{\Delta}|$ is the distance between the quark and the spectator in A.

Although $U(z_{\perp})$ modifies the transverse momentum of the quarks, the integrated cross section

$$\frac{d\sigma_{DY}}{dQ^2 dx_F} = \int_0^1 \frac{dx}{x} \int d^2 z_{\perp} \tilde{\psi}_A^{\dagger}(x, z_{\perp}) U^{\dagger}(z_{\perp}) \frac{d\sigma(q\bar{q} \rightarrow \mu\bar{\mu})}{dQ^2 dx_F} U(z_{\perp}) \tilde{\psi}_A(x, z_{\perp}) \quad (2.6)$$

is unchanged from (2.2) for Abelian initial state interactions, since then $U^{\dagger} d\sigma U = d\sigma U^{\dagger}U = d\sigma$. This is evident order by order in perturbation theory, where, for example, the contribution from the diagram in Fig. 8a cancels that from Fig. 8b. The situation is quite different for color (or flavor) changing initial state collisions (due to gluon exchange for example). In that case the potential V in (2.5b) is an Hermitian color matrix, and the eikonal phase a unitary color matrix. While $U^{\dagger}U$ still equals unity, the U 's do not in general commute with $d\sigma(q\bar{q} \rightarrow \mu\bar{\mu})$ in (2.6). The annihilating quark and anti-quark colors are not longer uncorrelated. For example, the diagrams in Fig. 8 would cancel except that they have different color factors when colored gluons are exchanged (i.e., C_F^2/n_c and $C_F(C_F - C_A/2)/n_c$). Because of the color factors, the diagrams in Fig. 8b add to those in Fig. 8a thereby enhancing the cross section. Crossed ladder diagrams and tri-gluon couplings do not contribute to the leading order eikonal potential (in Coulomb gauge).

In a general Drell-Yan process $AB \rightarrow \mu\bar{\mu}X$, the eikonal potential in (2.5b) includes interactions between all pairs of constituents, one taken from each of A and B — i.e., active-spectator (as above), active-active,¹³ and spectator-spectator interactions (Fig. 9a):¹⁴

$$V = \sum_{\substack{i \in A \\ j \in B}} V_{ij} (\vec{z}_{\perp i} - \vec{z}_{\perp j} + \vec{\Delta}_{\tau}) \quad , \quad (2.7)$$

where the impact parameters $z_{\perp i}$ are measured relative to the annihilation point. Of course, the interaction is not just Coulombic, even in perturbation theory. The complete leading order (in g^2) potential is due to both Coulomb and transverse gluon exchanges — the latter giving a contribution identical to the Coulomb interaction in leading order. Beyond leading order, the real part of the full constituent-constituent amplitude (e.g., Fig. 9b) contributes with $V_{ij} \sim (1/s)\text{Re } T_{ij}$. (Note that only amplitudes that grow like $T \sim s$ contribute as $s \rightarrow \infty$. Such behavior is associated with vector exchange; e.g., T is constant for a scalar gluon, so that V vanishes as $1/s$. The eikonal phase is energy dependent when T/s is not constant.) Also, inelastic amplitudes, such as in Fig. 9c, must be included in the eikonal potential. Therefore U is not only a unitary matrix in color space, but in Fock space as well; it can create and destroy spectators. Only inelastic interactions that leave the longitudinal momentum of the active quarks essentially unchanged eikonalize, and only these are included in U . Thus, the particles created or destroyed by these interactions are all in the central region — i.e., $j^- \sim j^+ \sim |j_{\perp}| \sim |k_{\perp}|$ for the diagram in Fig. 9c. Hard bremsstrahlung from the annihilating quark lines must be treated separately. It is discussed in the next section.

The potentials in sum (2.7) tend to cancel for large τ (i.e., large longitudinal separation) since hadrons A and B are color singlets.¹⁵ Of course, they do not cancel in general when τ is of the order or less than the transverse size $\langle z_{\perp} \rangle$ of A or B, and this is where the dominant contribution arises.¹⁶ Given the extreme Lorentz contraction of the beam and target particles, it is surprising that interactions occur at such large longitudinal distances ($\sim \langle z_{\perp} \rangle$), even in an Abelian theory. However,

this is an essential feature of eikonal interactions, which transfer only limited longitudinal momentum ($|\ell_3| \lesssim \ell_\perp \ll \sqrt{s}$), and consequently have only limited longitudinal resolution ($\Delta z \gtrsim 1/\ell_\perp \gg 1/\sqrt{s}$). In fact, as we show in Appendix A, the collinear Ward identities used in conventional analyses of Drell-Yan are valid for any interaction (in any gauge) with $|\ell_3| \gg \ell_\perp^2/P$, so that the only interactions carrying $|\ell_3| \lesssim \ell_\perp^2/P$ are relevant to the new physics we are discussing. Thus the eikonal interaction is actually non-zero (and roughly constant) over a range $\langle z_\perp \rangle^2 \sqrt{s}$ — much longer even than the range in our Coulomb gauge analysis above. The Coulomb gauge analysis can be corrected by using collinear Ward identities to alter the potential:¹⁷

$$\frac{g^2}{\ell^2} \rightarrow \frac{g^2}{\ell_\perp^2} \theta(|\ell_3| \lesssim \ell_\perp^2/P) \quad , \quad (2.8)$$

but only $\ell_3 \approx 0$ contributes in Eq. (2.4) anyway, so that the final result is unchanged as $s \rightarrow \infty$. (In the limit $s \rightarrow \infty$ the target is Lorentz contracted to a size $L_T M/\sqrt{s}$, so that the reduction of the range of the eikonal potential in Coulomb gauge has no physical consequences. For example, the contribution from $\ell_\perp^2/P \ll |\ell_3| \lesssim |\ell_\perp|$ in Eq. (2.3) is suppressed by a factor $\sim M L_T \ell_\perp^2/s$ because of the approximate asymmetry of the integrand under $\ell^3 \rightarrow -\ell^3$.) Use of Ward identities can be avoided completely by computing in axial gauges like $A^3 = 0$ gauge. For these only $|\ell_3| \lesssim \ell_\perp^2/P$ contributes although the calculations are somewhat more involved than in Coulomb gauge (see Appendix B).

The physical origins of such long range interactions are discussed in Appendix B. Their consequences are important for nuclear targets. Because of the long range, constituents throughout the entire nucleus contribute to the eikonal phase.¹⁸ This leads to novel A dependence in

the normalization, Q_{\perp} distribution, and associated multiplicity (central region). In particular we do not expect cross sections that scale exactly as A^1 . However, the deviation from A^1 behavior may be small, both because of Sudakov suppression of $d\sigma_8$, and because any diagram involving interactions with a spectator nucleon is suppressed by a color factor $\sim 1/n_c^2 = 1/9$ relative to the diagrams that contain only interactions with constituents of the annihilation nucleon. The A dependence could be modified in a large nucleus, since the net change in the eikonal potential is of relative order $A^{1/3}/n_c^2$.

Finally, we note that the approximations leading from Eq. (2.3) to Eq. (2.4), and ultimately to the full eikonal formalism, are valid only at high energies. Essentially, we are neglecting the longitudinal momentum ℓ_3 transferred to the active quarks in comparison to the 'uncertainty' in the momentum they already carry. For a nuclear target, ℓ_3 of order $A^{1/3} \langle \ell_{\perp} \rangle \equiv A^{1/3} \lambda$ is lost when central region particles are produced by multiple interactions of the sort shown in Fig. 9c. This is negligible provided that $|\ell_3| L_N(M_N/P_N) \ll 1$, where $L_N(M_N/P_N)$ is the Lorentz contracted length of the hadrons within which each of the active quarks is confined. Thus we require that

$$A^{2/3} \lambda^2 (M_N L_N)^2 \ll s_N \quad (2.9)$$

(where $s_N \equiv s/A$ is the energy per hadron in the CM frame), if the wave functions of the active quarks are to remain coherent along the length of the annihilation region. Otherwise the Drell-Yan cross section is reduced. Notice that this condition also insures that the active quarks lose only a small fraction of their energy to spectators and central region particles. This is an obvious requirement in an eikonal analysis.

III. BREMSSTRAHLUNG

As we have seen in Section II, multiple elastic collisions leave the longitudinal momentum distributions of the active quarks essentially unaffected. Using the notion of longitudinal flux conservation, one can then understand easily why elastic collisions in an Abelian theory have no effect on the integrated Drell-Yan cross section. However, one might expect bremsstrahlung, induced by collisions between active and spectator quarks, to carry off a finite fraction of active quarks' longitudinal momentum, thereby drastically altering the pair-production cross section — even in the Abelian case. In fact, as we shall show, the effects of all hard radiation (with momentum $j_{\perp}^2 \gg \ell_{\perp}^2$) can be completely absorbed into the $q\bar{q}$ cross section in Eq. (2.6) — i.e., we replace $d\sigma(q\bar{q} \rightarrow \mu\bar{\mu})$ by $d\sigma_H(q\bar{q} \rightarrow \mu\bar{\mu}X)$ where all real and virtual radiative corrections are hard. On the other hand, all soft radiation ($j_{\perp} \lesssim \ell_{\perp}$) must occur well before any initial state interactions, and is included with the spectators in the hadronic wavefunctions; soft radiation occurring between initial state collisions is suppressed at large Q^2 for all but the longest targets. Bremsstrahlung occurring in the central region of the rapidity distribution contributes both to the eikonal operator and to $d\sigma_H(q\bar{q} \rightarrow \mu\bar{\mu}X)$.

A. Real Emission

In order to illustrate the techniques we employ in treating initial state bremsstrahlung, we consider the lowest order graphs for quark + meson $\rightarrow \mu\bar{\mu}$ + transverse gluon + X, shown in Fig. 10. Once again, we use time-ordered perturbation in the center-of-mass frame. We then obtain the following expressions for the energy denominators:

$$A \simeq \frac{1}{2P} \left[-\frac{j_{\perp}^2}{z(1-z)} + i\epsilon \right] \quad (3.1)$$

$$B \simeq \frac{1}{2P} \left[-4y P^2 - \frac{j_{\perp}^2}{z(1-z+y)} - \frac{\ell_{\perp}^2 - 2\ell_{\perp} \cdot j_{\perp}}{1-z+y} - \frac{(k_{\perp} - \ell_{\perp})^2}{1+y} - \frac{k_{\perp}^2}{1-x} + i\epsilon \right]$$

$$C \simeq \frac{1}{2P} \left[-4y P^2 - \frac{\ell_{\perp}^2}{1+y} - \frac{(k_{\perp} - \ell_{\perp})^2}{x+y} - \frac{k_{\perp}^2}{1-x} + i\epsilon \right]$$

— valid when masses are negligible, $y < x$, $1 - z$ and $j_{\perp}^2, \ell_{\perp}^2, k_{\perp}^2 \ll P^2$.

Here y and z are the longitudinal momentum fractions: $y = \ell^3/P$, $z = j^3/P$.

To leading order in $1/P$, the bremsstrahlung gluon simply couples to the quark convection current, which is $\vec{J}^q = (-j_{\perp}, (2-z)P) + \mathcal{O}(\ell_{\perp}, yP)$ for each diagram in Fig. 10. Since the polarization vector is orthogonal to the gluon's momentum (j_{\perp}, zP) in Coulomb gauge, the gluon-quark vertex is typically

$$\vec{\epsilon} \cdot \vec{J}^q \simeq -\frac{2\epsilon_{\perp} \cdot j_{\perp}}{z} + \mathcal{O}(\ell_{\perp}, yP) \quad (3.2)$$

The exchanged gluon, carrying momentum \vec{k} , gives the same factor (g^2/\vec{k}^2) for each diagram when one includes the energy flux factors $1/(2E)$ for the intermediate states.

It is convenient here to consider large j_{\perp} ($\gg \ell_{\perp}$) separately from small j_{\perp} ($\lesssim \ell_{\perp}$).¹⁹ We treat each region in turn for the graphs in Fig. 10. We also examine contributions from central-region radiation.

Large j_{\perp} . As usual, one can make use of the collinear Ward identities to absorb the contribution from the region $|y| \gtrsim \ell_{\perp}^2/P^2$ into the structure functions (see Section II and Appendix A). For the remaining region,

$|y| \lesssim \ell_{\perp}^2/P^2$, it is obvious from Eqs. (3.1) and (3.2) that only diagram (b) of those in Fig. 10 contributes to leading order in $1/s$ for $j^2 \gg \ell_{\perp}^2$.²⁰

In the large j_{\perp} region, the denominator B and the gluon-quark vertex

$\vec{\epsilon} \cdot \vec{j}^q$ are independent of \vec{k} . Furthermore, the denominator C is independent of \vec{j} . Thus the \vec{k} integration decouples in this region, and the amplitude factors into the product of an initial state interaction and a radiative correction to pair production.

Following Ref. 1,²¹ it can be shown that this factorization occurs in Coulomb gauge for $s \rightarrow \infty$ even if one does not use the Ward identities to eliminate contributions from the region $k^2/P^2 \ll |y| \lesssim k_{\perp}/P$. As explained in Section II, this region does not contribute for targets that are sufficiently Lorentz contracted in the CM frame.

Small j_{\perp} . For $j^2 \lesssim k_{\perp}^2$, graphs in which the gluon emission occurs before all initial state interactions (e.g., Figs. 10a and 10c) can be treated as contributions from the higher Fock state components of the active quark's wavefunction. The emitted gluon plays the role of a spectator constituent. Thus, Fig. 10c actually represents a spectator-spectator interaction in this region. Graphs in which the gluon emission occurs between an initial state interaction and the annihilation vertex (e.g., Fig. 10b) tend to be suppressed because of a cancellation between contributions from eikonal denominators on either side of the gluon emission vertex.

Let us demonstrate this cancellation for the graph in Fig. 10b. The important contributions at large s come from the eikonal region, where $|y| \lesssim k_{\perp}^2/P^2$. In this region, the energy denominators for diagram (b) can be written as (Eq. (3.1))

$$\begin{aligned} B &\approx (-y - y_B + i\epsilon) s/2P \\ C &\approx (-y - y_C + i\epsilon) s/2P \end{aligned} \quad , \quad (3.3)$$

with $y_B - y_C \approx M^2/s$, where M is the invariant mass of the quark gluon system ($M^2 \sim j_{\perp}^2/(z(1-z)) \lesssim \ell_{\perp}^2$). Then the contribution from Fig. 10b is of the form (see Eq. (2.4))

$$\frac{M_H}{x} \int dy d^2 \ell_{\perp} \frac{1}{-y-y_C+i\epsilon} \frac{\vec{\epsilon} \cdot \vec{j}^q}{s} \frac{1}{-y-y_B+i\epsilon} \frac{g^2}{\ell^2} \psi_A(x+y, k_{\perp} - \ell_{\perp}) . \quad (3.4a)$$

This amplitude can be written as the difference of two terms, one corresponding to gluon emission induced by the initial state interaction, and the other to gluon emission induced by the annihilation:

$$\frac{M_H}{x} \int dy d^2 \ell_{\perp} \left\{ \frac{1}{-y-y_B+i\epsilon} - \frac{1}{-y-y_C+i\epsilon} \right\} \frac{\vec{\epsilon} \cdot \vec{j}^q}{M^2} \frac{g^2}{\ell^2} \psi_A(x+y, k_{\perp} - \ell_{\perp}) , \quad (3.4b)$$

where we have used $y_B - y_C \approx M^2/s$. These two processes interfere destructively, and they cancel completely when the wavefunction is insensitive to shifts of order $(y_B - y_C)P \sim \ell_{\perp}^2/P$ in the longitudinal momentum carried by the annihilating anti-quark.²² By the uncertainty principle, we see that this is the case provided that $\Delta k^3 (L_T M_T/P) \ll 1$, where $\Delta k^3 = (y_B - y_C)P$ is the shift in the longitudinal momentum and $L_T M_T/P$ is the Lorentz contracted length of the target in the center-of-mass frame.

Thus no bremsstrahlung occurs when

$$\langle \ell_{\perp}^2 \rangle L_T M_T \ll s . \quad (3.5)$$

If condition (3.5) is satisfied, there is insufficient time between the initial state collision and the annihilation to generate a soft gluon.²³ On the other hand, additional radiation can occur if (3.5) is not satisfied. Indeed, radiation must occur as a hadron passes through a long (macroscopic) target, and, as a consequence, the incident beam is depleted and secondary hadron beams are produced.

For nuclear targets, condition (3.5) can be rewritten (see also (1.8)):

$$\begin{aligned}
 Q^2 \gg x M_N L_A \langle \ell_{\perp}^2 \rangle_A &\sim x M_N (1.4 \text{ Fm}) A^{1/3} \lambda^2 A^{1/3} \\
 &\sim x A^{2/3} (0.6 \text{ GeV}^2) \quad , \quad (3.6)
 \end{aligned}$$

where $\lambda \sim 100\text{--}500$ MeV is the momentum exchanged per initial state collision. Thus for uranium one might require $Q^2 > x 24 \text{ GeV}^2$ before radiative losses within the nucleus can be neglected. In general, the commonly used parameterization $d\sigma_A = A^\alpha d\sigma_N$ for the Drell-Yan cross section is consistent with (3.6) only if α varies both with Q^2 and A .

Central-Region Radiation. The diagram in Fig. 10b does contribute for small $j_{\perp} (\lesssim \ell_{\perp})$ when the radiated gluon is in the central region of the rapidity distribution — i.e., $j^3 \sim j_{\perp} \sim \ell_{\perp}$. Then $|y_B - y_C| \sim j_{\perp}^2 / (zs)$ can become large and the two terms in Eq. (3.4b) need not cancel. However, we see from Eq. (3.4b) that the radiated gluon is associated partly with the initial state interaction, in which case it contributes to the eikonal operator (since $z \lesssim \ell_{\perp} / P$), and partly with the annihilation, in which case it contributes to the radiative corrections to $d\sigma_H(q\bar{q} \rightarrow \mu\bar{\mu}X)$. This analysis is easily generalized in higher orders. Thus all effects due to central-region radiation can be incorporated into the eikonal operator and the $q\bar{q}$ annihilation cross section.

B. Virtual Corrections to $d\sigma_H(q\bar{q} \rightarrow \mu\bar{\mu}X)$

The analysis of virtual loop corrections to the $q\bar{q}$ subprocess follows closely that of real emission. For the purposes of illustration, we consider the graph shown in Fig. 11a. Just as for real emission (Fig. 10b), the j and ℓ integrations decouple in the large j_{\perp}^2 region

($j_{\perp}^2 \gg \lambda^2$), and the amplitude factors into the product of an initial state interaction and a (virtual) radiative correction to pair production. The contribution from small j_{\perp}^2 ($\lesssim \lambda^2$) is already included in the eikonal operator described in Section II; in this region, Fig. 11a corresponds to an active-spectator eikonal interaction followed by an active-active eikonal interaction.

Diagrams such as those in Fig. 11b contribute only in the eikonal region and so are analyzed as in Section II. Diagrams in which quarks or gluons within the same hadron interact (e.g., Fig. 11c) vanish for large s when one adds the Coulomb and transverse gluon contributions. The analysis for these diagrams is similar to that leading up to Eq. (3.4b). The conclusion is that there is insufficient time for the (time-dilated) internal interactions to occur during the collision.

C. Sudakov Logarithms

Thus far we have shown that the amplitude for emission of real and virtual gluons in the presence of initial state interactions can be factored into the form of an initial state matrix phase times ordinary radiative corrections to the Drell-Yan amplitude. This factorization is valid for emitted gluon momenta $|j_{\perp}| > \lambda_A$. Since, in the factored form, the initial state color matrix appears to the outside of the ordinary QCD radiative corrections, the color factors associated with real emission are different from those associated with virtual emission. As a consequence, the usual infrared cancellation of large double logarithms (Sudakov logarithms) between real and virtual emission graphs fails in a non-Abelian theory.

Let us examine these double logarithms in some detail for the order α_s radiative corrections shown in Fig. 12. In general, the double logarithms arise as follows: one logarithm comes from the "infrared region" $|\vec{j}| \approx 0$; a second logarithm comes from one of the "collinear regions" $p \cdot j = P(|\vec{j}| - j_3) \approx 0$ or $p' \cdot j = P(|\vec{j}| + j_3) \approx 0$ (in the case of virtual emission one takes the residue at the gluon pole at $j^0 = |j|$). In the Coulomb gauge, the Coulomb gluons never contribute to the double logarithms, since they are absent in the case of real emission, and they contain no pole at $j = |\vec{j}|$ in the case of virtual emission. In the CM frame, the leading part of the coupling of the quark currents to the transverse gluon polarization sum is

$$J_i J_k \left(\delta_{ik} - \frac{j_i j_k}{j^2} \right) \approx \pm \frac{4P^2}{j^2} (|\vec{j}| - j_3)(|\vec{j}| + j_3) \quad , \quad (3.7)$$

where the plus sign applies to the graphs of Fig. 12 (b,c,f,g) and the minus sign to the graphs of Fig. 12 (a,d,e). Since the numerator factor (3.7) cancels the quark propagator denominators $p \cdot j$ and $p' \cdot j$ that become singular in the "collinear region," the vertex corrections (Fig. 12a) and the graphs involving real emission from different quark lines (Figs. 12d and 12e) cannot contribute a double logarithm. Real emission graphs in which the transverse gluon attaches to the same quark at each end (Figs. 12f and 12g) contain the square of one of the singular quark propagators, and so contribute a collinear as well as an infrared logarithm. Neglecting color factors, one finds that the double logarithmic contribution of the graphs of Figs. 12f and 12g is

$$d\sigma^{f,g} = \frac{2\alpha_s}{4\pi} \ln^2 \left(\frac{Q^2}{\lambda_A^2} \right) d\sigma_0 \quad . \quad (3.8a)$$

If we take into account the running of the coupling constant, one of these logarithms is changed to a $\ln \ln$:

$$d\sigma^{f,g} = \frac{2}{\beta_0} F(Q^2) d\sigma_0 \quad . \quad (3.8b)$$

where

$$F(Q^2) = \ln \left(\frac{\ln Q^2/\Lambda^2}{\ln \lambda_A^2/\Lambda^2} \right) \ln \left(Q^2/\lambda_A^2 \right) \quad .$$

A self-energy correction (Figs. 12b and 12c) can also contribute collinear logarithms, since subtracting the δm^2 piece of the amplitude results in the squaring of the quark propagator. Neglecting color factors and taking into account the running of the coupling constant, one finds that the self-energy graphs give a double logarithmic contribution

$$d\sigma^{b,c} = -\frac{2}{\beta_0} F(Q^2) d\sigma_0 \quad . \quad (3.9)$$

In an Abelian theory, the double logarithms in (3.8) and (3.9) would cancel. However, as was first pointed out by Mueller,⁸ in the presence of color-carrying initial state interactions, the color factor associated with Figs. 12b and 12c is different from the color factor associated with Figs. 12f and 12g, and the cancellation fails. More precisely, these graphs give cancelling contributions to $d\sigma_1$:

$$d\sigma_1^{b,c} = -d\sigma_1^{f,g} = \left(-n_c + \frac{1}{n_c} \right) \frac{1}{\beta_0} F(Q^2) \quad ; \quad (3.10)$$

however, in $d\sigma_8$, the radiation part is suppressed relative to the real emission part:

$$d\sigma_8^{b,c} = \left(n_c^2 - 1 \right) d\sigma_8^{f,g} = \left(-n_c + \frac{1}{n_c} \right) \frac{1}{\beta_0} F(Q^2) \quad . \quad (3.11)$$

Thus there is a residual contribution to $d\sigma_8$

$$d\sigma_8^{b,c,f,g} = - \frac{C_A}{\beta_0} F(Q^2) d\sigma_0 \quad . \quad (3.12)$$

$$(C_A = n_c) \quad .$$

Sudakov form factors have been studied extensively to all orders in perturbation theory for both Abelian and non-Abelian theories.²⁴ The leading double-log terms, such as in Eq. (3.12), exponentiate to give

$$d\sigma_8 \sim \exp \left\{ - \frac{C_A}{\beta_0} F(Q^2) \right\} d\sigma_0 \quad . \quad (3.13)$$

The double-log terms cancel in $d\sigma_1$. Assuming that perturbation theory gives the correct asymptotic behavior as $Q^2 \rightarrow \infty$, we conclude that $d\sigma_8$ is suppressed at large Q^2 relative to $d\sigma_1$ by a Sudakov form factor:

$$d\sigma_8 \sim \exp \left\{ - \frac{C_A}{\beta_0} \ell n \left(\frac{\ell n Q^2/\Lambda^2}{\ell n \lambda_A^2/\Lambda^2} \right) \ell n \frac{Q^2}{\lambda_A^2} \right\} d\sigma_1 \quad . \quad (3.14)$$

IV. OTHER APPLICATIONS OF INITIAL AND FINAL STATE INTERACTIONS

The canonical factorized form for hard scattering inclusive cross sections,²⁵

$$d\sigma = \int \prod G(x_i, Q) d\hat{\sigma} D(x_j, Q) dx_i dx_j \quad (4.1)$$

has played a central role in the analyses of perturbative QCD predictions for the whole range of deep inelastic and large momentum transfer inclusive reactions. The analyses of this paper show that Eq. (4.1) is in general modified by the effects of initial and/or final state interactions of the hadrons. In QCD perturbation theory these gauge invariant leading order (in $1/s$) contributions are due to soft gluon exchange and emission and can be organized into unitary eikonal matrix phases

$$\begin{aligned}
 U_{\text{ISI}}(z_{\perp}^i) &= P_{\tau} \exp \left[-i \int_{-\infty}^0 d\tau U_{\text{ISI}}(\vec{z}_{\perp}^i + \vec{\Delta}\tau) \right] \\
 U_{\text{FSI}}(z_{\perp}^j) &= P_{\tau} \exp \left[-i \int_0^{\infty} d\tau U_{\text{FSI}}(\vec{z}_{\perp}^j + \vec{\Delta}\tau) \right] ,
 \end{aligned}
 \tag{4.2}$$

where the Hermitian potentials U_{ISI} and U_{FSI} are constructed (as in Eq. (2.7)) from the sum of interactions of all pairs of quark and gluon constituents of the interacting hadrons. These generalized potentials include all irreducible contributions to the scattering amplitude that scale with s , including (in Coulomb gauge in the CM system) Coulomb and transverse gluon exchange, crossed graph contributions, and the inelastic contributions that create (or destroy) quarks or gluons of finite momentum in the CM. The essential contributions come from the region of near-on-shell constituent propagation and finite momentum transfer in the CM—precisely the kinematic regime where the collinear Ward identities required for proving factorization are inapplicable.

Thus, Eq. (4.1) is replaced by

$$\left| U_{\text{ISI}}(z_{\perp}^i) \mathcal{M} U_{\text{FSI}}^{\dagger}(z_{\perp}^j) \right|^2$$

convolved with the wavefunctions $\psi(z_{\perp}^i, \mathbf{x}^i)$ of the initial and final state hadrons. For cases in which the final state hadrons are unobserved, as in deep inelastic lepton-hadron scattering, the final state interactions give no correction to the cross section as $s \rightarrow \infty$ because of unitarity:

$$U_{\text{FSI}}^{\dagger}(z_{\perp}^j) U_{\text{FSI}}(z_{\perp}^j) = 1 \quad . \tag{4.3}$$

However, the initial and final state interactions do, in general, modify the transverse momentum distributions of the interacting constituents (giving a contribution in addition to that due to the hadron Fock state wavefunctions $\psi(\mathbf{x}^i, \mathbf{k}_{\perp}^i)$), and lead to the production of associated particles

in the central rapidity region. Most important, the initial state interactions due to colored vector gluon exchange introduce color correlations which, order by order in perturbation theory, modify the normalization of virtually every inclusive QCD cross section involving two incident hadrons. As in the Drell-Yan cross section, the eikonal color matrix U does not, in general commute with the hard-scattering QCD cross section:

$$U_{|S|} d\hat{\sigma} U_{|S|}^\dagger \neq d\hat{\sigma} \quad . \quad (4.4)$$

Again, just as in the Drell-Yan analyses, the real and virtual hard gluon radiative corrections to the subprocess cross section summed to all orders lead to asymptotic Sudakov damping of the color correlation effects. However, for subasymptotic momentum transfer, one has not only a renormalization of each inclusive cross section involving incident hadrons, but also a new source of QCD scale breaking beyond that given by standard evolution of the structure and fragmentation functions.

The color correlation effects may be largest for processes such as $gg \rightarrow \chi$, $gg \rightarrow \eta_c$, which have strong color suppression in lowest order. The lowest order color factor for these processes, $1/(n_c^2 - 1) = 1/8$, could be increased by a factor as large as 64. The normalizations of leading twist subprocesses for high p_T hadron and photon production are also modified by the initial state color factors.

Although our analysis is based on QCD perturbation theory (to all orders) our conclusions can be expressed in terms of rather general principles:

1. Critical Momentum Scale. The characteristic momentum of each hard subprocess must be large compared to a scale set by the length of the target (or beam), as in Eq. (3.5); otherwise the constituents, in passing through the target can lose a significant fraction of their longitudinal

momentum' to radiation, completely destroying any connection between the hadronic reaction and the distributions measured in deep inelastic scattering. This is related to the more general concept of the formation zone.

2. Formation Zone. The state of a hadronic system cannot be modified significantly in a time (in its rest system) less than its intrinsic scale. Thus, a high energy quark cannot radiate a collinear gluon $q \rightarrow q + g$ inside of a target of length L if $s \gg \Delta(\mathcal{M}^2)LM$ where $\Delta(\mathcal{M}^2)$ is the change in the square of the invariant mass, and LM/s is proportional to the Lorentz contracted length of the target in the quark rest frame. Similarly, the fragmentation of a quark into collinear hadrons (or vice versa) occurs outside of the target volume at high energies. We also note that interactions between quark or gluon constituents of the same hadron do not occur (to leading order in $1/s$) during the transit through the target volume. Thus high energy interactions of hadrons within nuclei are correctly described in terms of constituent quark and gluon propagation.

3. Large Longitudinal Range. As we have discussed in Section II, the change of longitudinal momentum (in the CM) due to initial or final state interactions is so small that longitudinal structure in the target cannot be resolved in a target of length $L < \sqrt{s}/\langle \ell_{\perp}^2 \rangle$ (as measured in the CM frame). In particular, this implies that the color correlation factors can have non-trivial nuclear target dependence.

4. Color Singlet Cancellations. Large momentum transfer exclusive reactions are controlled by the Fock states with the minimum number of constituents at transverse distances $b_{\perp}^2 \sim (1/Q^2)$.²⁶ The initial and final state collisions can probe transverse distances no smaller than $1/\lambda$. Thus, they cannot resolve the internal structure of the hadrons in exclusive

reactions, and they do not couple to these color neutral objects. Formally, the initial and final state interactions cancel to leading order in $1/Q^2$ if one adds the contributions coming from all constituents of a color neutral hadron. This also implies that large momentum transfer quasi-elastic reactions such as $eA \rightarrow ep(A-1)$ and $\pi A \rightarrow \pi p(A-1)$ can occur deep inside a nuclear target without multiple scattering or bremsstrahlung in the target.²⁷ Color singlet cancellations also eliminate initial and final state interactions of hadrons interacting directly in hard scattering inclusive reactions. For example, the "direct pion" has no initial state interactions in $\pi_D g \rightarrow q\bar{q}$ (in $\pi p \rightarrow q\bar{q}X$),²⁸ and no final state interactions in $gq \rightarrow \pi_D q$ (in $pp \rightarrow \pi X$).²⁹ Similarly, the higher twist $F_L \sim 1/Q^2$ contribution to the meson structure function³⁰ is unaffected by initial and final state interactions. On the other hand, although they are power law suppressed at large momentum transfer, the initial and final state interactions are expected to play an important role at moderate kinematic values, possibly leading to non-trivial helicity and interference effects. A part of the difference between time-like and space-like form factors, e.g., $e^+e^- \rightarrow \pi^+\pi^-$ and $e^-\pi^+ \rightarrow e^-\pi^+$ is attributable to final state interactions, although the difference is suppressed by $\sim 1/Q^2$.

Virtually every large momentum transfer inclusive process in QCD is affected by initial and/or final state interactions. It is important to study the phenomenology of these interactions since they bear on the dynamics of quarks and gluons in hadronic matter and are evidently related to the confinement mechanisms and the space-time "inside-outside" development of QCD jets.³¹ Analysis of the role played by nuclear targets is clearly crucial to this study.

In the remainder of this section we describe briefly some specific applications of the analysis of initial and final state interactions. A more detailed discussion will be given in a separate paper.

A. Deep Inelastic Lepton-hadron Scattering

Although the structure function measurements are unaffected by initial and final state interactions, the development of the final state jet distribution is modified by multiple scattering in the target. The transverse momentum of the struck quark relative to the current direction is broadened and multiplicity in the central region is increased, thus affecting the fragmentation distribution of quarks into hadrons $D_{H/q}(z, k_{\perp})$. (The k_{\perp} smearing that appears here is not identical to that which affects incident quarks in the Drell-Yan process.) These effects should increase with the number of collisions in a nuclear target:

$$\delta \langle k_{\perp}^2 \rangle \propto A^{1/3} \quad , \quad \delta \langle n_{\text{central}} \rangle \propto A^{1/3} \quad . \quad (4.5)$$

In addition, for long targets, energy-momentum conservation implies a correlated degradation of the leading particle distribution at large z . For low quark energies, collinear radiation can be induced in the target and can drastically alter the longitudinal momentum fraction distributions.

The development of hadronic multiplicity in deep inelastic lepton scattering³² in the nucleus is particularly interesting, since one is studying the influence of hadronic matter on quark jet propagation. As we have emphasized, formation of leading particles occurs outside the nuclear volume at high energies. The inelastic final state interactions amount to cascading in the nucleus and demonstrate that, contrary to the usual assumptions made for the analysis of hadron-nucleus collisions, particle

production in the target and central rapidity region cannot be correlated with the number of nucleons "wounded" by the beam. A model for the shape of the rapidity distribution based on "color cascading" is given in Ref. 33.

More generally any hard scattering inclusive process is accompanied by soft hadrons in the central rapidity region, which are the result of the initial state or final state interactions of the quark and gluon constituents. We emphasize that, even though the hard scattering cross section can be computed as if a single interaction occurs, the associated multiplicity distribution reflects the full scope of the actual QCD dynamics.

B. Hadron Production at Large Transverse Momentum

In addition to the change in normalization of the heading twist subprocess due to color correlations, hadron production at large transverse momentum in a nucleon or nuclear target collision is increased by the k_{\perp} smearing effects of the initial and final state interactions. The multiple scattering series in a nucleus³⁴ leads to terms roughly of order A^1 , $A^{4/3}/p_{\perp}^2$, $A^{5/3}/p_{\perp}^4$, etc. A coefficient of the A^{α} terms with $\alpha > 1$ can be very large, since one is smearing a cross section that falls very rapidly with p_{\perp} . Thus, strongly suppressed cross sections such as $pA \rightarrow \bar{p}X$ and $pA \rightarrow K^-X$ obtain a much larger nuclear enhancement from quark and gluon scattering effects than channels such as $pA \rightarrow \pi^+X$ or $pA \rightarrow K^+X$. In the case of direct γ production $pA \rightarrow \gamma X$, the photon has no final state interactions, so only initial state interactions of the active q and g constituents are important. Similarly, at large x_T where direct subprocesses such as $gq \rightarrow \pi_D q$ or $qq \rightarrow \pi_D g$ are expected to dominate $pA \rightarrow \pi X$ production, only initial state interactions are important.

The nuclear initial and final state effects are, of course, enhanced in processes such as $A_1 A_2 \rightarrow HX$. Nuclear targets also enhance the effects of multiple scattering processes that lead to multiple jets in the final state.³⁵ On the other hand, if the valence state of a hadron consists of constituents at small transverse distances, then the hadron can pass through the target with no color or hadronic interactions. An application of this idea to diffractive dissociation processes in nuclei is discussed by G. Bertsch et al. (Ref. 27).

Processes such as $pp \rightarrow pp\mu\bar{\mu}$,³⁶ which occur via $\gamma\gamma \rightarrow \mu\bar{\mu}$ subprocesses, are also sensitive to the nature of initial state interactions. Unlike the corresponding lepton-induced reaction $ee \rightarrow ee\mu\bar{\mu}$, the initial state interactions of the two nucleons smear the transverse momentum distribution of the $\mu\bar{\mu}$ pair and can eliminate the strong peaking at $Q_{\perp} = 0$ associated with the γ poles. However, the cross section integrated over all Q_{\perp} is unchanged.

Finally, we note that the techniques we have discussed in this paper can be used to analyze the shadowing behavior of structure functions in the low x , low Q^2 domain. Details will be presented in a separate paper.

ACKNOWLEDGEMENTS

We wish to thank J. Collins, T. Jaroszewicz, A. Mueller, D. Soper, G. Sterman, and D. Yennie for helpful conversations.

APPENDIX A

COLLINEAR WARD IDENTITIES AND THE EIKONAL POTENTIAL

It is instructive to compare the calculation of initial state effects in Coulomb gauge (Section II) with that in Feynman gauge. Consider, for example, the diagram in Fig. 13a, where, as in Section II, the momenta are $P_q = (P, 0_\perp, P)$ and $P_A = (P, 0_\perp, -P)$. In Feynman gauge, unlike Coulomb gauge, this amplitude has leading contributions from the entire collinear region — i.e., from $0 \lesssim |y| = |\ell^3/P| \lesssim 1$, where the gluon carries an appreciable fraction of the target's longitudinal momentum. Such terms are usually simplified by noting that the gluon couples to the top (beam) quark line only through the $\gamma^+ = \gamma^0 + \gamma^3$ vertex, since $\bar{u}(\vec{P}_q + \vec{\ell}) \gamma^+ u(P_q) \sim 2P \gg \bar{u} \gamma^- u, \bar{u} \gamma_\perp u$. This gluon coupling can then be replaced by $2\ell/\ell^-$ to leading order in $1/s$, and the ordinary Ward identities can be used to move the gluon vertex to the annihilation point (Fig. 13b):

$$\begin{aligned} \dots \frac{1}{\not{P}_q + \not{\ell}} \gamma^+ u(\vec{P}_q) &\approx \dots \frac{1}{\not{P}_q + \not{\ell}} \frac{2\ell}{\ell^-} u(\vec{P}_q) \\ &= \dots \frac{2}{\ell^-} u(\vec{P}_q) \end{aligned} \quad (A.1)$$

In this way, ℓ is decoupled from P_q , and the collinear contribution can be absorbed into a redefinition of the target's structure function — just as in deep inelastic scattering. This sort of Ward identity can be used for any graphs containing initial state exchanges. In particular, it applies to the initial state interactions with gluon bremsstrahlung discussed in Section III (Fig. 10). Notice, however, that the substitution $\gamma^+ \rightarrow 2\ell/\ell^-$ in Eq. (A.1) is valid only if $\ell^- \gg \ell_\perp^2/P_q^+ = \ell_\perp^2/2P$ — i.e., if $\bar{u}(\vec{P}_q + \vec{\ell}) \gamma^+ u(\vec{P}_q) \approx \bar{u}(\vec{P}_q + \vec{\ell}) 2\ell/\ell^- u(\vec{P}_q)$. Similarly, contributions from

$\ell^+ \gg \ell_{\perp}^2/P_A^- = \ell_{\perp}^2/2P$ can always be absorbed into the beam quark's structure function. The region $\ell^+, \ell^- \lesssim \ell_{\perp}^2/P$ must be treated separately. Our central observation is that interactions carrying infinitesimal ℓ^+ and ℓ^- still contribute to leading order in $1/s$, due to singularities in the energy denominators. These singularities arise from the possibility of on-shell propagation between interactions. Thus, the collinear contributions can be factored in the usual fashion, but the eikonal contributions lead to a variety of new phenomena.

The differences between Drell-Yan and deep inelastic scattering become apparent if we restrict our attention to gluon momenta in the eikonal region, $\ell^+, \ell^- \lesssim \ell_{\perp}^2/P$ (in any gauge). In second order, for example, the eikonal contributions to these processes come only from uncrossed ladder diagrams as in Fig. 14a,b. Although important in the collinear region, crossed-ladder and tri-gluon diagrams (Fig. 14c,d) are pure imaginary (if non-zero) in this order, and so do not contribute in the eikonal region. The color factors for diagrams a and b are the same for deep-inelastic scattering, resulting in complete cancellation of eikonal corrections to the structure function. However, the color factors differ in Drell-Yan, leading to an enhancement of the cross section. The difference here is simply that final state eikonal interactions always cancel (by unitarity), and initial state eikonal interactions do not cancel for processes like Drell-Yan.

The use of Ward identities to restrict the momentum transferred by eikonal interactions is not arbitrary. The collinear region $\ell^+, \ell^- \gg \ell_{\perp}^2/P$ gives identical contributions to the Drell-Yan and deep-inelastic cross sections. Thus, one can define the hadronic wave functions so that

they contain all such collinear contributions. (Indeed, one must absorb all collinear (mass) singularities into the wave functions in order to factor the deep-inelastic scattering cross section.) Then, only those eikonal interactions that come from the region ℓ^+ , $\ell^- \lesssim \ell_{\perp}^2/P$ remain. The eikonal potential is gauge invariant, since the eikonal region is by definition the region in which intermediate states are almost exactly on-shell, and on-shell amplitudes are gauge invariant. This is also true for more complicated interactions. For example, the eikonal part of the diagram in Fig. 15 comes from $|\ell_1^-| \lesssim \ell_{\perp}^2/P_q^+$, $|\ell_2^+| \lesssim \ell_{\perp}^2/P_A^-$ and j in the central region (i.e., $j_{P_A}^{+-} \sim j_{P_q}^{-+} \sim j_{\perp} \sqrt{s}$).³⁷

It is suggested in Ref. 10 that the ℓ^3 integration contour for terms such as those in Eq. (2.4) be deformed so as to avoid completely the eikonal region. It is then argued that collinear Ward identities apply to the entire contribution. However, the contour deformation is inconsistent with the collinear Ward identities when, for example, radiation is included in non-Abelian theories. In particular, diagrams like that in Fig. 16a, involving tri-gluon couplings, require a contour deformation different from the others (Fig. 16b) if the eikonal region is to be avoided. The contour deformation differs because energy denominators in the non-Abelian Feynman diagrams contain poles that are on the opposite side of the real ℓ^3 axis from those in the Abelian diagrams. This is because the non-Abelian diagrams actually include both initial state and final state interactions (Fig. 16a). Both are needed to make up the complete Feynman amplitude, and, thus, both are needed in order to employ the collinear Ward identities.

A problem closely related to questions of contour deformation and use of collinear Ward identities is the treatment of initial state interactions between spectators. Such interactions give important contributions to the eikonal phase in non-Abelian theories. We note that the expressions presented in Ref. 10 are incomplete in that they do not take into account the spectator-spectator interactions.

APPENDIX B

THE RANGE OF THE EIKONAL POTENTIAL, AND ZITTERBEWEGUNG

The preceding discussion of collinear Ward identities (Appendix A) demonstrates that elastic eikonal interactions can carry only

$$\ell^- \lesssim \ell_{\perp}^2 / P_q^+ \quad \ell^+ \lesssim \ell_{\perp}^2 / xP_A^- \quad (\text{B.1})$$

in $qA \rightarrow \mu\bar{X}$. Consequently these initial state interactions can resolve longitudinal structure at distances of order $\sqrt{s}/\langle\ell_{\perp}^2\rangle$ or larger in the center of mass frame ($P_q^+ = P_A^- = \sqrt{s}$). In particular the beam quark is completely insensitive to the longitudinal structure of any nuclear target smaller than $\sim s/(\langle\ell_{\perp}^2\rangle M)$ (in the target's rest frame). This seems paradoxical, even in the Abelian case, since the electric and magnetic fields of the quarks and gluons in the target are strongly Lorentz contracted in the longitudinal direction. Thus one might expect the beam quark to interact with only one nucleon at a time, starting at the front face of the nucleus and finishing at the annihilation point. In fact, our analysis shows that it interacts simultaneously with the entire nucleus, including those nucleons located after the annihilation point. The difference between these pictures is not academic. In the first scenario, only interactions in the annihilation nucleon would contribute to the color correlation, and the cross section would still scale as A^1 . In reality, interactions with the entire nucleus contribute, and, in a non-Abelian theory, the A dependence could be modified.

This phenomenon is most easily understood in the rest frame of the beam quark ($P_q^+ = m$, $P_A^- = s/m$). There the position of the beam quark can at best be specified only to within a Compton wavelength³⁸ due to the zitterbewegung, resulting in an effective potential with a range of order

the Compton wavelength. This is precisely the range implied by the inequalities (B.1), which, in the projectile rest frame, become $|\lambda^3| \lesssim \langle \lambda_{\perp}^2 \rangle / m$, where $m \sim \sqrt{\langle \lambda_{\perp} \rangle}$ is the effective quark mass in a hadron.³⁹ Thus, in this frame, the longitudinal resolution of the eikonal potential is $\sim 1/m$. The target nucleus, being Lorentz contracted by Mm/s , is usually much shorter than this range.

It is interesting that the effective eikonal potential can be obtained directly in gauge theories by making a suitable choice of gauge. For a charged particle moving at the speed of light in the z direction, the electric and magnetic fields are completely Lorentz contracted in that direction. That is,

$$E_{\perp} \rightarrow \frac{g}{2\pi} \frac{r_{\perp}}{|r_{\perp}|^2} \delta(z-vt) \quad , \quad E_{\parallel} \rightarrow 0 \quad (B.2)$$

$$\vec{B} = \vec{v} \times \vec{E}$$

as $v \rightarrow 1$ in an Abelian theory. However, the vector potential in a physical gauge such as $A^3 = 0$ gauge has a long range⁴⁰ - i.e.,

$$A_{\perp} \rightarrow \frac{1}{v} \frac{g}{4\pi} \frac{r_{\perp}}{|r_{\perp}|^2} \epsilon(z-vt) \quad , \quad A^0 \rightarrow A^3 = 0 \quad , \quad (B.3)$$

where $\epsilon(z) = \pm 1$ for $\pm z > 0$. It is the vector potential, not the \vec{E} and \vec{B} fields, that is relevant to the quantum mechanical behavior of the beam quark.

This discussion provides a new insight into the nature of collinear Ward identities. Intuitively, one expects initial and/or final state interactions in the Drell-Yan process and in deep inelastic scattering.

However, due to zitterbewegung, the only physically relevant interactions of this type are long range - i.e., those that transfer limited longitudinal momentum (Eq. (B.1)). Thus it must be true that we can absorb any initial or final state interaction transferring large momentum into a redefinition of the structure functions. This is what is accomplished via collinear Ward identities. But the zitterbewegung argument tells us that such a redefinition of structure functions must also be possible in non-gauge theories. That is, the algebraic manipulations used in implementing Ward identities are not unique to gauge theories; they apply to any initial or final state interaction. This is easily illustrated for interactions due to a scalar gluon, although the eikonal potential is suppressed in that case by $1/s$. Gauge theories are unique in that the gauge freedom can be exploited to eliminate the large momentum contributions to the eikonal potential from the beginning.

REFERENCES AND FOOTNOTES

¹G. T. Bodwin, S. J. Brodsky and G. P. Lepage, Phys. Rev. Lett. 47, 1799 (1981); and in the Proceedings of the 1981 Banff Summer School on Particles and Fields, edited by A. N. Kamal and A. Capri (Plenum Press, 1982). A report on this work was also presented in S. J. Brodsky et al., in "Perturbative Quantum Chromodynamics," edited by D. W. Duke and J. F. Owens (AIP Conference Proceedings No. 74, 1981), Proceedings of the Tallahassee Conference, March 1981.

²S. D. Drell and T. M. Yan, Phys. Rev. Lett. 25, 316 (1970). Possible complications in the parton model prediction due to "wee parton" exchange are discussed in this paper.

³H. D. Politzer, Nucl. Phys. B 129, 301 (1977); R. K. Ellis, H. Georgi, M. Machacek, H. D. Politzer and G. C. Ross, Nucl. Phys. B 152, 285 (1979); S. Gupta and A. H. Mueller, Phys. Rev. D 20, 118 (1979). A discussion of final state interactions and possible problems with factorization for the Drell-Yan process is given in J. C. Collins and D. E. Soper, Proceedings of the Moriond Workshop, Les Arcs, France (1981).

⁴Possible nuclear effects on transverse momentum have also been considered by C. Michael and G. Wilk, Zeit. Phys. C 10, 169 (1981). See also T. Jaroszewicz and M. Jezabek, Zeit. Phys. C 4, 277 (1980); and A. Bialas and E. Bialas, Phys. Rev. D 21, 675 (1980).

⁵G. E. Hogan, Ph.D. Dissertation, Princeton University (1979).

⁶See, for example, Hung Cheng and Tai Tsun Wu, Phys. Rev. D 1, 2775 (1970). An eikonal model for the effects of soft-scattering for large transverse momentum in nuclei has been given by Paul M. Fishbane and J. S. Trefil, Phys. Rev. D 12, 2113 (1975).

⁷Only the colors of the annihilating quark and anti-quark are important here. If together they are in the color singlet state, then $d\sigma_{\text{eff}} = (1/n_c)d\sigma_1 + (n_c - 1/n_c)d\sigma_8$. If they are in any of the eight color octet states, then $d\sigma_{\text{eff}} = (1/n_c)(d\sigma_1 - d\sigma_8)$. In general the quark and anti-quark are in some mixture of these nine states where $\cos^2\theta$ is the probability of finding the singlet state. When the quark colors are uncorrelated, each of the nine states occurs with equal probability and therefore $\cos^2\theta = 1/n_c^2 = 1/9$ (which leads to Eq. (1.4)). If one allows only pure active-spectator exchanges, it is easy to show that the requirement of unitarity leads to the condition $\cos^2\theta \geq 1/n_c^2$, so the cross section is always enhanced.

⁸A. H. Mueller, Phys. Lett. 108B, 365 (1982).

⁹Time ordered perturbation theory in this frame is somewhat similar to time ordered perturbation theory in the infinite momentum frame. See, for example, S. J. Brodsky, R. Roskies and R. Suaya, Phys. Rev. D 8, 4574 (1973).

¹⁰J. Collins, D. Soper and G. Sterman, Phys. Lett. 109B, 388 (1982).

¹¹The wavefunction used in Eq. (2.1) specifies the relative momenta of the constituents of A at a given time. Such an "equal-time" wavefunction becomes identical to the "light-cone" wavefunction, defined at a given $z^- = t - z$, in the limit $P_A^- = 2P \rightarrow \infty$. The equal-time wavefunction is obtained in this limit by replacing k^- by $-2k^3$ in the light-cone wavefunction. In fact, the light-cone wavefunction is the most natural in all frames, including the target's rest frame, since the beam quark probes the wavefunction at a particular z^- (the classical trajectory of the beam quark is $z^- \simeq \text{constant}$ as $s \rightarrow \infty$). The analysis is manifestly invariant under longitudinal boosts only when one uses the light-cone wavefunction.

Light-cone wavefunctions appear naturally when one makes use of light-cone perturbation theory, as in Ref. 1, but the analysis is then somewhat more complicated. The wavefunction used in Ref. 1 equals $\psi_A(x, k_\perp) / \sqrt{x(1-x)}$ in the infinite momentum frame. Further discussion of light-cone wavefunctions can be found in G. P. Lepage and S. J. Brodsky, Phys. Rev. D 22, 2157 (1980); and in the Proceedings of the 1981 Banff Summer School on Particles and Fields, edited by A. Kamal and A. Capri (Plenum Press, 1982).

¹²R. J. Glauber in Lectures in Theoretical Physics, edited by W. E. Brittin and L. G. Dunham, Wiley Interscience (New York), Vol. I, 315 (1959).

¹³The active-active interactions result in an ultra-violet divergence in the eikonal phase, because, in this case, the hadronic wave function does not limit the transverse momentum exchanged. However, one can factor this divergence out of the path-ordered eikonal operator U , since it occurs only at $\tau \approx 0$. The infinite part of the phase factor can be shown easily to cancel in both Abelian and non-Abelian theories.

¹⁴Abelian spectator-spectator interactions have been shown previously to cancel. See J. L. Cardy and G. A. Winbow, Phys. Lett. 52B, 95 (1974); and C. E. DeTar, S. D. Ellis and P. V. Landshoff, Nucl. Phys. B 87, 176 (1975).

¹⁵The potentials cancel completely for $|\tau| \gg |z_{\perp 1}|$ in an Abelian theory, and the eikonal phase is infrared finite - spectator-spectator and active-active interactions cancel the infrared divergences in the active-spectator interaction. In non-Abelian theories, this cancellation works only for the first gluon exchanged. Thereafter the hadrons (in intermediate states) need no longer be color singlets. However, the first interaction occurs at most a distance \sqrt{s}/λ^2 (i.e., the effective range

of the eikonal interaction) from the annihilation point, due to the partial infrared cancellation. Thus the infrared divergences are regulated in perturbation theory in non-Abelian theories by an s -dependent cutoff (i.e., \sqrt{s}/λ^2), rather than the typical hadronic size $\langle z_{\perp} \rangle$, which acts as the cutoff in Abelian theories. This would lead to an energy independent eikonal phase. However, the infrared divergences in QCD are probably cut off by (s -independent) non-perturbative effects. We wish to thank T. Jaroszewicz for discussions on this point.

¹⁶Indeed, hadrons have no transverse size for QCD in two dimensions, and the initial state interactions cancel in the large n_c limit. See J. Kripfganz and M. G. Schmidt, Nucl. Phys. B 125, 323 (1977); and also J. H. Weis, Acta Phys. Pol. B 9, 1051 (1978).

¹⁷By employing collinear Ward identities, we determine the true upper limit of the longitudinal momentum transferred by the eikonal interactions. For simplicity, we represent the limitation by a θ -function in the eikonal potential. In fact, the cutoff in ℓ_3 is not so abrupt. For example, if we replace $(-2\ell_3 - \Delta + i\epsilon)^{-1}$ by $\mathcal{P}(-2\ell_3)^{-1}$ in the energy denominator of Eq. (2.3), then this contribution can be eliminated for all ℓ_3 by use of the collinear Ward identities. Thus, the eikonal contribution is obtained by taking the difference of these denominators: $(-2\ell_3 - \Delta + i\epsilon)^{-1} \rightarrow (-2\ell_3 - \Delta + i\epsilon)^{-1} - \mathcal{P}(-2\ell_3)^{-1} = (-2\ell_3 - \Delta + i\epsilon)^{-1} \mathcal{P}(\Delta/-2\ell_3)$. The effective eikonal potential is then $(g^2/\vec{\ell}^2) \mathcal{P}(\Delta/-2\ell_3)$, which contributes only for $\ell_3 \sim \Delta \sim \ell_{\perp}^2/P$. This is precisely the sort of potential that is obtained in $A^3 = 0$ gauge.

¹⁸Spectators separated from the annihilation point by a longitudinal distance greater than the range of the eikonal potential cannot affect the color correlation of the active quarks. This is because the path ordering

in Eq. (2.5b) allows us to factor interactions with such spectators out of the eikonal operator, in which case they cancel in $d\sigma/dx_F dQ^2$. Thus only those particles within range of the annihilation point can affect the normalization. However, this generally includes the entire target nucleus at high energies.

¹⁹The large- j_{\perp} region corresponds to the range over which the "j-parts" of Ref. 1 give the dominant contributions. In the small- j_{\perp} region, the "k-parts" also become important. Here we find it most convenient to define the "j-parts" to be zero in the small- j_{\perp} region, since the characteristic "j-part" structure is not dominant there.

²⁰For simplicity, we have made approximations in Eq. (3.1) that are valid only for $j_{\perp}^2 \ll P^2$. In fact, this region gives the dominant contribution for large j_{\perp}^2 . However, as can be seen by examining the exact energy denominators, our discussion is valid for $j_{\perp}^2 \sim P^2$ as well.

²¹The approach of Ref. 1 is based on the following argument. Diagrams (a) and (b) in Fig. 10 give identical contributions for $j_{\perp}^2 \gg k_{\perp}^2$, except for their color factors. Taken together they have the same color factor as diagram (b). All three diagrams can be combined by noting that the energy denominators are approximated by

$$A \approx \frac{1}{2P} \left[- \frac{j_{\perp}^2}{z(1-z)} + i\epsilon \right]$$

$$C \approx \frac{1}{2P} \left[- 4 yP^2 + i\epsilon \right]$$

$$B \approx C + A$$

in this region, so that

$$\frac{1}{AB} + \frac{1}{BC} = \frac{1}{AC} \quad .$$

A is the denominator associated with emission of a gluon and C the denominator associated with elastic active-spectator scattering. Thus, by combining the graphs with all orderings of gluon emission and active-spectator scattering, one again obtains an amplitude that factors.

²²For example, $\psi(x+y) \sim e^{i(x+y)LM}$ is the wavefunction for constituents at fixed separation L in the rest frame. For sufficiently large L, the phase of ψ varies rapidly with changing y and the cancellation in (3.4b) is destroyed. In the opposite limit, $L \rightarrow 0$, the wavefunction becomes constant and the cancellation is obvious.

²³This result can be understood another way. As discussed in Footnote 11, the collision takes place at a particular $z^- = t - z$ and, for long targets, over a range $\Delta z^+ \sim L_T M_T / P$. Thus only gluons with wavelength $\lambda^+ \lesssim \Delta z^+$ can be generated during the collision - i.e., gluons with $j^- = j_1^2 / zP \lesssim 1 / \Delta z^+ \sim P / L_T M_T$ are not radiated. This is just condition (3.5). This argument is very similar to the discussion of the "formation zone" for radiation due to a classical current given by L. Landau and I. Pomeranchuk, Doklady Akademii Nauk SSSR 92, 535 (1953). We thank L. Stodolsky for bringing this work to our attention.

²⁴See A. Sen, Phys. Rev. D 24, 3281 (1981) and references therein.

²⁵A. H. Mueller, Phys. Rep. 73, 238 (1981).

²⁶G. P. Lepage and S. J. Brodsky, Phys. Rev. D 22, 2157 (1980) and references therein.

²⁷This has been discussed by A. H. Mueller, to be published in Proceedings of the Moriond Conference (1982). Applications to elastic hadron-nucleus amplitudes are given in S. J. Brodsky and B. T. Chertok, Phys. Rev. Lett. 37, 269 (1976). Color singlet cancellations for

valence states interacting inclusively in nuclei are discussed in G. Bertsch, S. J. Brodsky, A. S. Goldhaber and J. F. Gunion, Phys. Rev. Lett. 47, 297 (1981).

²⁸E. L. Berger and S. J. Brodsky, Phys. Rev. D 4, 2428 (1981).

²⁹E. L. Berger, P. Gottschalk and D. Sivers, Phys. Rev. D 23, 99 (1981). See also G. Farrar and G. C. Fox, Nucl. Phys. B 167, 205 (1980); and J. A. Bagger and J. F. Gunion, U.C. Davis preprint, UCD-81/3.

³⁰G. R. Farrar and D. R. Jackson, Phys. Rev. Lett. 35, 1460 (1975); and E. L. Berger and S. J. Brodsky, Phys. Rev. Lett. 42, 940 (1979).

³¹J. D. Bjorken, lecture notes in Current-Induced Reactions edited by J. Komer et al., Springer-Verlag (New York) 1975; J. Kogut and L. Susskind, Phys. Rev. D 10, 732 (1974).

³²For experimental data see L. Hand et al., Acta Phys. Pol. B 9, 1087 (1978); and H. C. Ballagh et al., Phys. Lett. 79B, 320 (1978).

³³S. J. Brodsky, SLAC-PUB-2395, also in Proceedings of the First Workshop on Nuclear Collisions, Berkeley (1979).

³⁴See J. Kuhn, Phys. Rev. D 13, 2948 (1976); and A. Krzywicki, J. Engels, B. Petersson and V. Sukhatme, Phys. Lett. 85B, 407 (1979).

³⁵N. Paver and D. Treleani, Trieste preprint, ISAS 7/82/EP (1982) and references therein.

³⁶F. Vanucci, Contribution to the Karlsruhe Summer Institute, Karlsruhe (1978).

³⁷This discussion also has bearing on the analysis of electron-electron scattering for $s \gg |t|$. For example, if one simply applies collinear Ward identities to the sum of all ladder and crossed ladder diagrams and ignores the eikonal region, their contributions seem to vanish. (This is because electron lines start and end on-shell, and the electrons are not

greatly deflected.) In fact, as is well known, the dominant contribution in this example comes only from the eikonal region ($\ell^\pm \lesssim |t|/\sqrt{s}$), and is leading order in $1/s$. This observation, an obvious consequence of the collinear Ward identities, is a critical element in the eikonal analysis of electron-electron, quark-quark, scattering, etc.

³⁸A massless particle confined to a finite region (i.e., inside a hadron) has an effective mass of order $1/L$, where L is the length of region. Its effective Compton wavelength is then of order L .

³⁹When masses are important, ℓ_\perp^2 is replaced by $\ell_\perp^2 + m^2$ in inequalities (B.1). The implications of zitterbewegung are less transparent in the target's rest frame. There it must be remembered that the beam quark probes the target's wavefunction at a fixed value of $z^- \equiv t - z$ (see Footnote 11). Thus the longitudinal structure of the target is specified by the $z^+ \equiv t + z$ dependence of its light-cone wavefunction. However, in this frame, the beam particle has a very long wavelength in the z^+ direction - $\lambda^+ \sim 1/P_q^+ \sim s(M_T(m_q^2 + \ell_\perp^2))^{-1}$ - and therefore the effective range of the eikonal potential again grows like s .

⁴⁰The range of the vector potential in $A^3 = 0$ gauge is infinite, even though our detailed calculations in this gauge show that the range of the eikonal potential is $O(\sqrt{s}/\lambda^2)$. This difference in ranges is an artifact of the singularity as $\ell^3 \rightarrow 0$ in the polarization sum for $A^3 = 0$ gauge. The singularity is regulated by making the replacement $(k^3)^{-n} \rightarrow 1/2 \{ (k^3 + i\delta)^{-n} + (k^3 - i\delta)^{-n} \}$ and taking $\delta \rightarrow 0$ at the end. Since the final results are finite as $\delta \rightarrow 0$, they are unchanged if δ is kept finite and sufficiently small. With this prescription, A_\perp in Eq. (B.3) is modified by a factor $e^{-|z - vt|\delta}$. Therefore, setting $\delta \sim \lambda^2/\sqrt{s}$ defines a

gauge in which the vector potential has the correct range even for s finite (but large).

FIGURE CAPTIONS

- Fig. 1. The conventional view of the Drell-Yan process.
- Fig. 2. Initial state interactions in the Drell-Yan process.
- Fig. 3. Chicago-Illinois-Princeton data for the mean square transverse momentum of a lepton pair produced in pion-nucleon collisions. M is the invariant mass of the pair.
- Fig. 4. The dominant color flow due to a single non-Abelian active-spectator interaction.
- Fig. 5. The general decomposition of the cross section $d\sigma(q\bar{q} \rightarrow \mu\bar{\mu}X)$ into color singlet and octet exchange pieces.
- Fig. 6. A Drell-Yan process which has a zero cross section unless there is an initial state interaction. Here a W -boson is exchanged.
- Fig. 7. Initial state corrections in $qA \rightarrow \mu\bar{\mu}X$.
- Fig. 8. Diagrams which cancel for Abelian interactions, but not for non-Abelian interactions.
- Fig. 9. Additional interactions contributing to the eikonal operator of Eq. (2.5b).
- Fig. 10. Examples of lowest-order contributions to the amplitude for real radiation with initial-state interactions in $qA \rightarrow \mu\bar{\mu}X$.

Fig. 11. Examples of lowest-order contributions to the amplitude for virtual radiation with initial state interactions in $qA \rightarrow \mu\bar{\mu}X$.

Fig. 12. Some $O(\alpha_s)$ radiative corrections to the Drell-Yan process.

Fig. 13. Collinear Ward identities for the Drell-Yan process.

Fig. 14. a,b) Diagrams having eikonal region contributions.

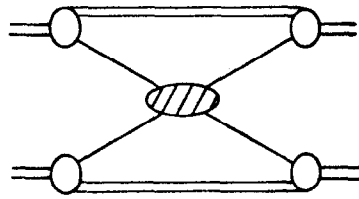
c,d) Diagrams that contribute only in the collinear region, if at all.

Fig. 15. Initial state interaction leading to particle production in the central region.

Fig. 16. a) Diagram including both initial and final state interactions.

b) Diagrams with only initial state interactions.

c) Diagrams with only final state interactions.



$$\begin{array}{c} \text{6-82} \end{array}
 \begin{array}{c} \diagdown \\ \diagup \end{array}
 \begin{array}{c} \text{shaded oval} \\ \diagup \\ \diagdown \end{array}
 =
 \begin{array}{c} \diagdown \\ \diagup \end{array}
 \begin{array}{c} \text{wavy line} \\ \diagup \\ \diagdown \end{array}
 \begin{array}{c} \text{vertical dashed line} \\ \diagup \\ \diagdown \end{array}
 \begin{array}{c} \text{wavy line} \\ \diagup \\ \diagdown \end{array}
 +
 \begin{array}{c} \diagdown \\ \diagup \end{array}
 \begin{array}{c} \text{wavy line} \\ \diagup \\ \diagdown \end{array}
 \begin{array}{c} \text{vertical dashed line} \\ \diagup \\ \diagdown \end{array}
 \begin{array}{c} \text{wavy line} \\ \diagup \\ \diagdown \end{array}
 + \dots
 \begin{array}{c} \text{4321A1} \end{array}$$

Fig. 1

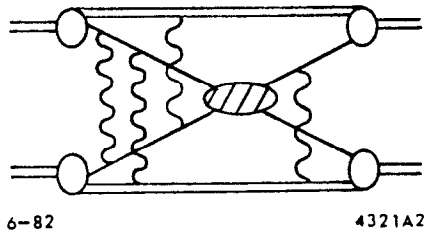


Fig. 2

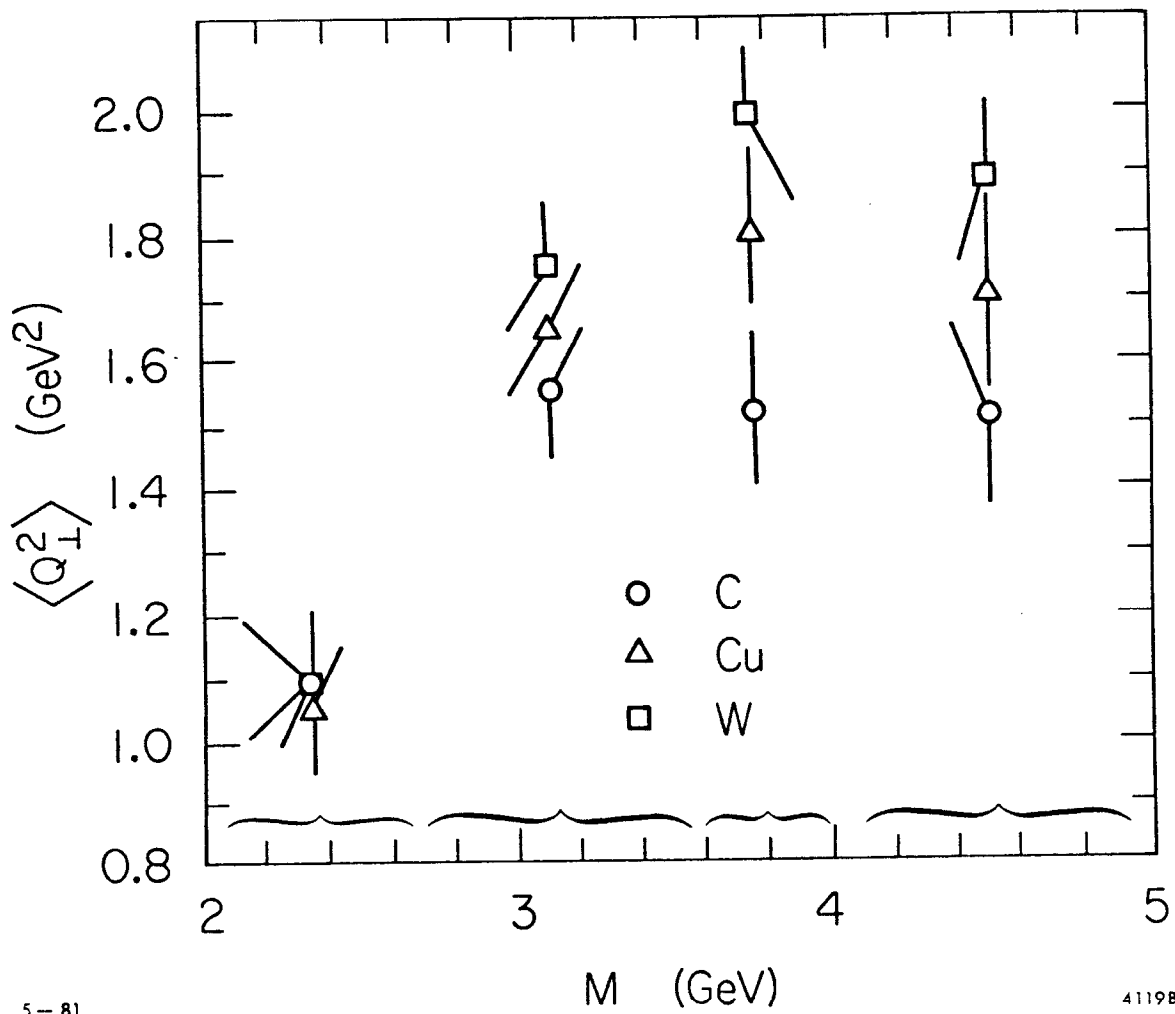
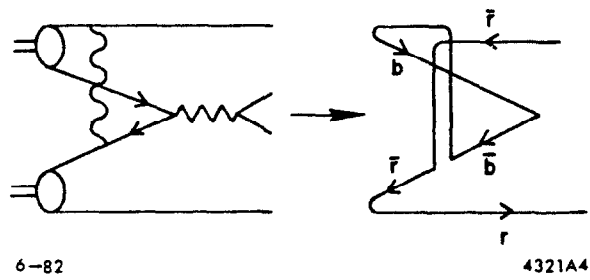


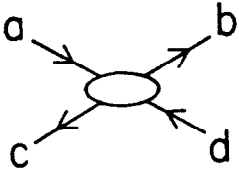
Fig. 3



6-82

4321A4

Fig. 4



$$\equiv \left(\frac{1}{n_c} \frac{a \rightarrow b}{c \leftarrow d} \right) d\sigma_1 + \left(2 \frac{a \rightarrow b}{c \leftarrow d} \right) d\sigma_8$$

6-82

4321A5

Fig. 5

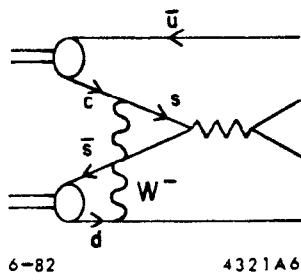
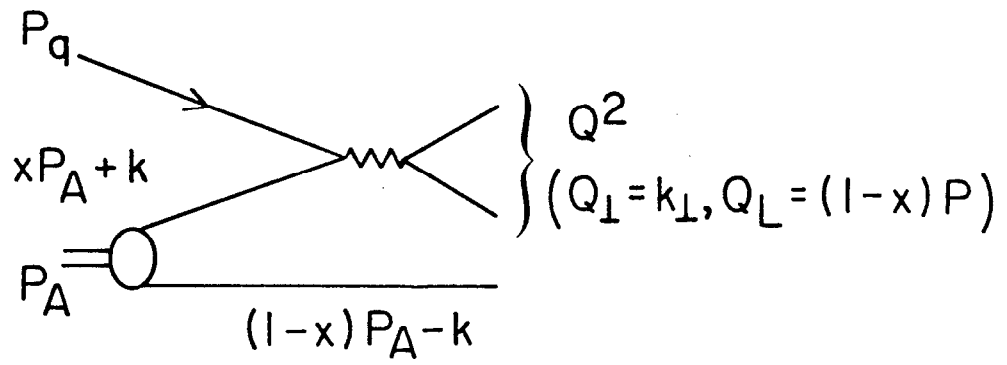
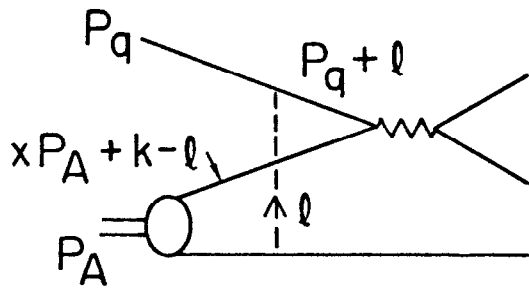


Fig. 6

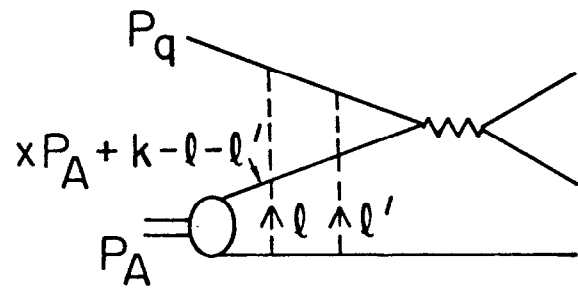


(a)



(b)

6-82

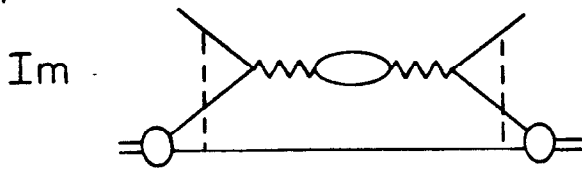


(c)

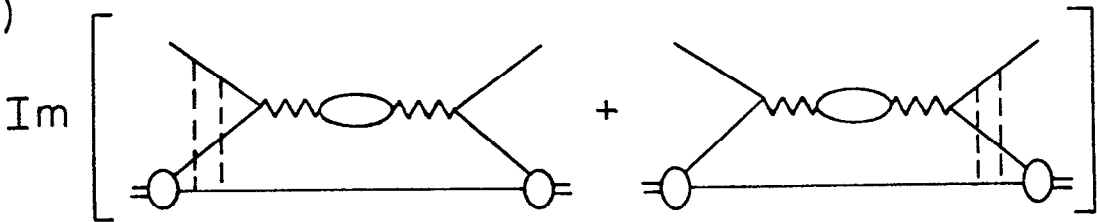
4321A7

Fig. 7

(a)



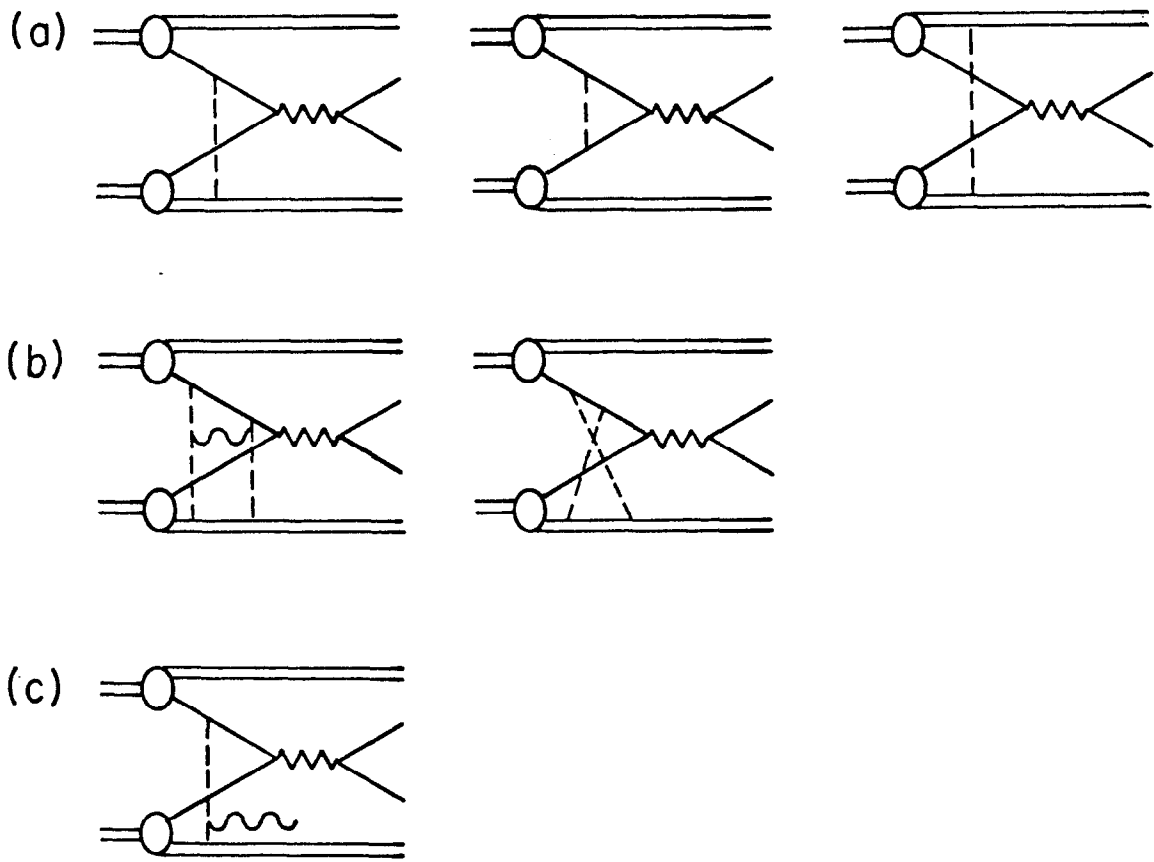
(b)



G-82

4321A8

Fig. 8



6-82
4321A9

Fig. 9

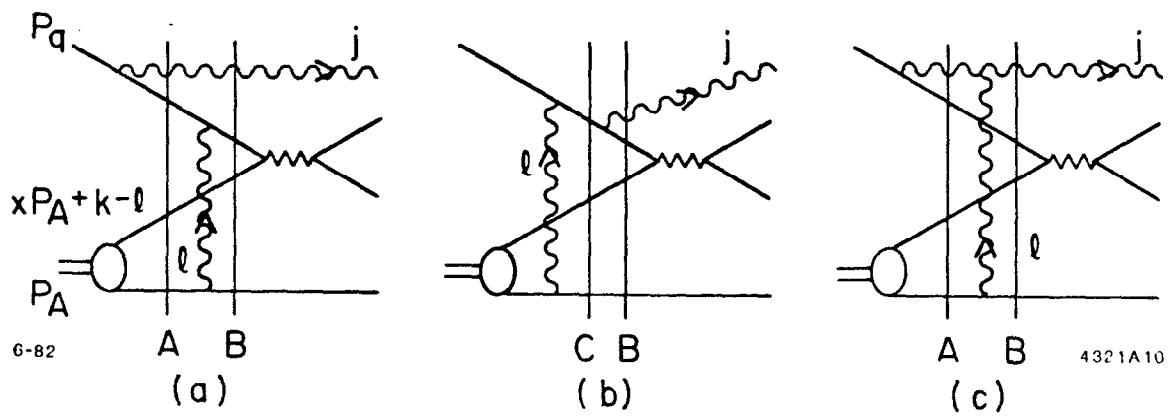
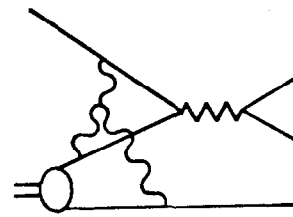
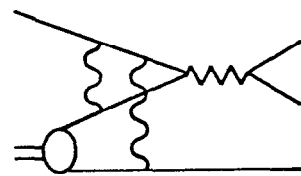
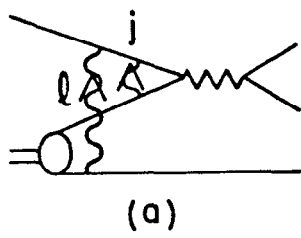
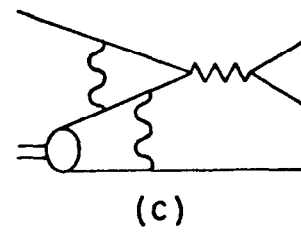


Fig. 10

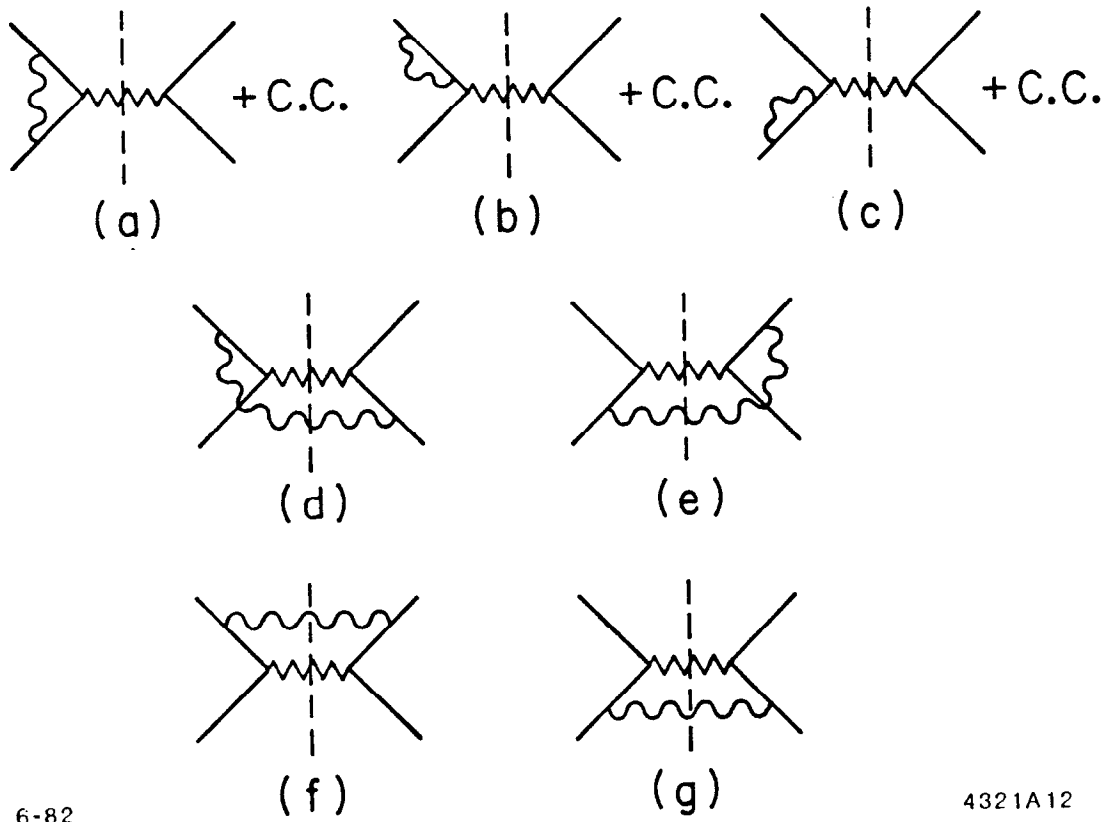


(b)



6-82
4321A11

Fig. 11



6-82

4321A12

Fig. 12

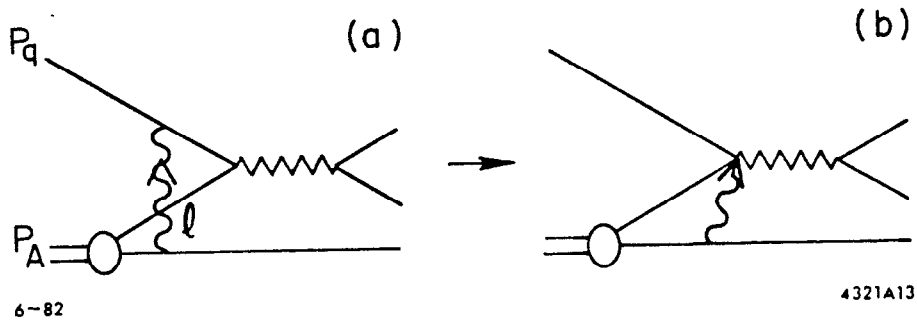
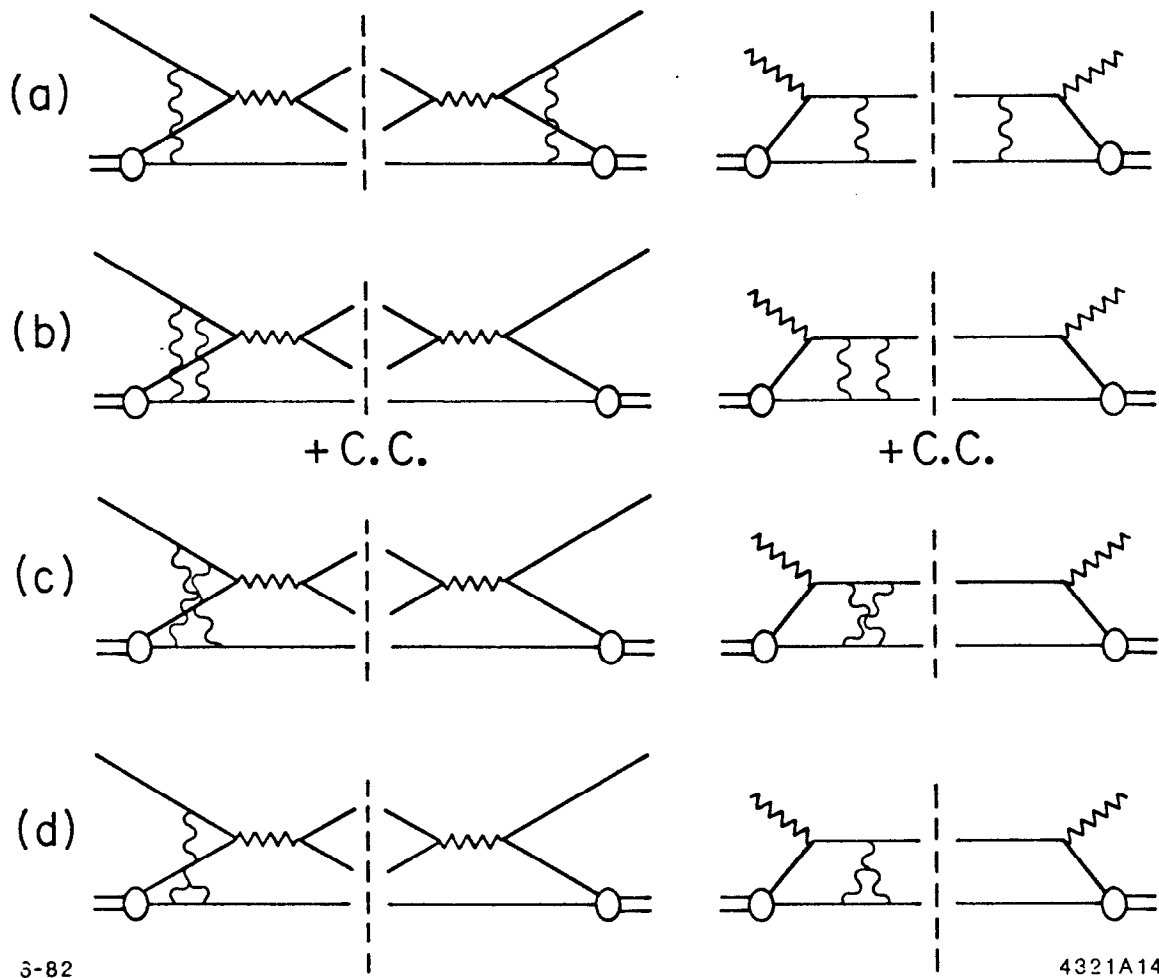


Fig. 13



3-82

4321A14

Fig. 14

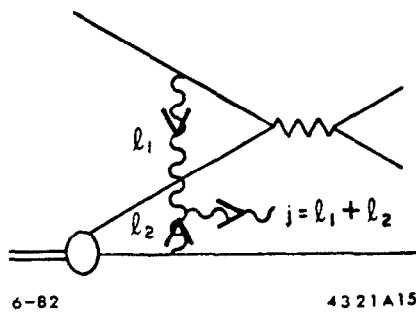
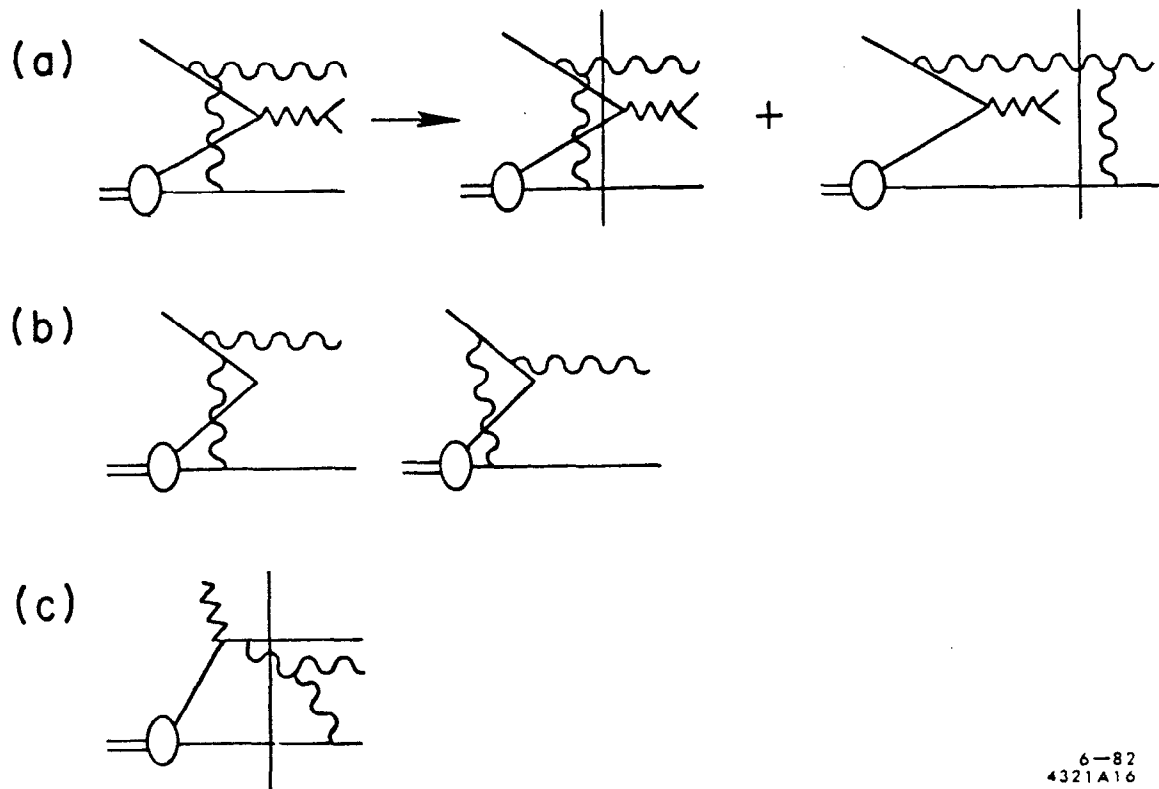


Fig. 15



6-82
4321A16

Fig. 16